FXR1P is a GSK3β substrate regulating mood and emotion processing

Thomas Del'Guidice[a], Camille Latapy[a,1], Antonio Rampino[b,1], Jivan Khlghatyan[a], Morgane Lemasson[a], Barbara Gelao[b], Tiziana Quarto[b,c], Giuseppe Rizzo[b], Annie Barbeau[a], Claude Lamarre[a], Alessandro Bertolino[b,d], Giuseppe Blasi[b], and Jean-Martin Beaulieu[a,2]

[a]Department of Psychiatry and Neuroscience, Faculty of Medicine, Université Laval, Québec-City, QC, Canada G1J 2G3; [b]Group of Psychiatric Neuroscience, Department of Basic Medical Science, Neuroscience and Sense Organs, University of Bari Aldo Moro, 70100 Bari, Italy; [c]Cognitive Brain Research Unit, Institute of Behavioral Sciences, University of Helsinki, 00014, Finland; and [d]Roche Innovation Center Basel, Hoffmann-La Roche, Ltd., 4070 Basel, Switzerland

Edited by Solomon H. Snyder, Johns Hopkins University School of Medicine, Baltimore, MD, and approved July 9, 2015 (received for review April 2, 2015)

Inhibition of glycogen synthase kinase 3β (GSK3β) is a shared action believed to be involved in the regulation of behavior by psychoactive drugs such as antipsychotics and mood stabilizers. However, little is known about the identity of the substrates through which GSK3β affects behavior. We identified fragile X mental retardation-related protein 1 (FXR1P), a RNA binding protein associated to genetic risk for schizophrenia, as a substrate for GSK3β. Phosphorylation of FXR1P by GSK3β is facilitated by prior phosphorylation by ERK2 and leads to its down-regulation. In contrast, behaviorally effective chronic mood stabilizer treatments in mice inhibit GSK3β and increase FXR1P levels. In line with this, overexpression of FXR1P in the mouse prefrontal cortex also leads to comparable mood-related responses. Furthermore, functional genetic polymorphisms affecting either FXR1P or GSK3β gene expression interact to regulate emotional brain responsiveness and stability in humans. These observations uncovered a GSK3β/FXR1P signaling pathway that contributes to regulating mood and emotion processing. Regulation of FXR1P by GSK3β also provides a mechanistic framework that may explain how inhibition of GSK3β can contribute to the regulation of mood by psychoactive drugs in mental illnesses such as bipolar disorder. Moreover, this pathway could potentially be implicated in other biological functions, such as inflammation and cell proliferation, in which FXR1P and GSK3 are known to play a role.

glycogen synthase kinase 3 | mood | emotion processing | FXR1P | bipolar disorder

Glycogen synthase kinase 3α and β (GSK3α/β) are two serine threonine kinases involved in myriads of biological functions ranging from metabolism to immunity and behavior (1, 2). In particular, several single nucleotide polymorphisms (SNPs) in the *GSK3B* locus or in genes involved in GSK3β signaling have been identified as genetic risk factors for bipolar disorder and schizophrenia (3, 4). In addition, GSK3β is inhibited—either directly or following its phosphorylation on Ser9 by AKT—in response to three major classes of psychiatric drugs that are mood stabilizers, antidepressants, and antipsychotics (5–10). Furthermore, pharmacological or genetic inhibition of GSK3β replicates behavioral effects of these drugs in rodents (11).

Because of its potential implication in mental disorders and their treatment, pharmacological inhibition of GSK3β has become an attractive therapeutic strategy for mental illnesses (12). However, several limitations associated to the selectivity and long-term toxicity of GSK3β inhibitors have remained serious obstacles (13, 14). One interesting alternative would be to target GSK3β substrates that are involved in the regulation of behavior by this kinase. However, the nature of these substrates has remained elusive, and evidence for their role in regulating behavior in humans is scarce.

An important layer of complexity for the identification of substrates involved in the regulation of behavior by GSK3β comes from the fact that GSK3β displays a 500–1,000-fold preference toward phosphoproteins (2, 15, 16). Indeed, most GSK3β substrates require prior phosphorylation to be phosphorylated by this kinase. This phenomenon, called "priming," results from the nature of the consensus amino acid sequence $S/T_1XXXpS/T_2$ that is recognized and phosphorylated by GSK3β. In this sequence, the amino-terminal S/T_1 corresponds to the serine or threonine that is phosphorylated by GSK3β, X is any amino acid, and pS/T_2 is the serine or threonine that acts as a priming site for GSK3β. Because of this need for priming, phosphorylation by GSK3β may therefore be highly context dependent and vary with changes of cell signaling landscapes that could be permissive or nonpermissive for the priming of a specific substrate.

Among the psychoactive drugs that affect GSK3β activity, mood stabilizers are a heterogeneous class of pharmacological agents used for the management of bipolar disorder as well as adjunct therapy for depression and schizophrenia. Lithium is the prototypical member of this class of psychiatric drugs that also includes the antiepileptic drugs lamotrigine and sodium valproate. Chronic administration of lithium, valproate, or lamotrigine has been shown to increase the inhibitory phosphorylation of GSK3β as a result of AKT activation (8, 17–20).

Regulation of GSK3β in response to mood stabilizers has several behavioral readouts that are not presently explained by the action of this kinase on any of its known substrates. Inhibition of

Significance

This study provides a cellular mechanism for the regulation of behavioral dimensions pertinent to mood disorders. Inhibition of glycogen synthase kinase 3β (GSK3β) is a shared action of drugs used for bipolar disorder. However, the substrates through which this kinase regulates mood are not known. We identified fragile X mental retardation-related protein 1 (FXR1P) as a substrate for GSK3β. Phosphorylation of FXR1P by GSK3β would lead to its down-regulation. Overexpression of FXR1P in the mouse prelimbic cortex elicits behavioral responses comparable to those of drugs inhibiting GSK3β. Furthermore, functional gene polymorphisms affecting FXR1P or GSK3β gene expression interact to regulate emotional brain responsiveness and stability in humans. These observations indicate that regulation of FXR1P by GSK3β contributes to regulating mood and emotion processing.

Author contributions: T.D., C. Latapy, A.R., J.K., M.L., C. Lamarre, and J.-M.B. designed research; T.D., C. Latapy, A.R., J.K., M.L., A. Barbeau, C. Lamarre, and J.-M.B. performed research; A.R., B.G., T.Q., G.R., A. Bertolino, G.B., and J.-M.B. contributed new reagents/analytic tools; T.D., C. Latapy, A.R., B.G., T.Q., G.R., A. Barbeau, and J.-M.B. analyzed data; and T.D., C. Latapy, A.R., A. Bertolino, G.B., and J.-M.B. wrote the paper.

The authors declare no conflict of interest.

This article is a PNAS Direct Submission.

Freely available online through the PNAS open access option.

[1]C. Latapy and A.R. contributed equally to this work.

[2]To whom correspondence should be addressed. Email: martin.beaulieu@crulrg.ulaval.ca.

This article contains supporting information online at www.pnas.org/lookup/suppl/doi:10.1073/pnas.1506491112/-/DCSupplemental.

exploratory locomotion is a known behavioral effect of GSK3β inhibition that is used to model "antimanic" effects (21, 22). Furthermore, lithium treatments and inhibition of GSK3β have been shown to exert an effect similar to antidepressants by reducing immobility in the tail suspension test (TST) (8, 23–25). Finally, lithium exerts GSK3β signaling-dependent effects similar to antidepressants and anxiolytics in the dark–light emergence test (DLET) (8, 24, 25). In this test, mice are placed in a darkened compartment and allowed free exploration of darkened and adjoining lighted compartments. Reduced latency to explore the light compartment as well as an increase in time and activity in this compartment are general indices of drug effect on mood-related behavior (26).

We identified two chronic treatments with sodium valproate (low-dose VAL 10 and high-dose VAL 25), which exhibit different behavioral effects in mice while resulting in comparable GSK3β inhibition. We have used this experimental paradigm to identify a substrate of GSK3β involved in the regulation of mood and emotions. This substrate, the fragile X mental retardation-related protein 1 (FXR1P), belongs to a small family of RNA binding proteins that also includes the fragile X mental retardation protein (FMRP) (27). Interestingly, SNPs in the *FXR1* gene have recently been identify as genetic risk factors for schizophrenia (28).

Our results indicate that FXR1P is down-regulated by GSK3β. Furthermore FXR1P is involved in the regulation of mood-related behaviors in mice, whereas genetic, brain imaging, and behavioral evidence obtained from healthy human subjects revealed a role of *GSK3B*/*FXR1* gene interactions in regulating emotional control. Taken together, these findings support a role of a GSK3β/FXR1P signaling pathway in regulating behavioral dimensions relevant to mood disorders in humans. Furthermore identification of a functional regulation of FXR1P by GSK3β suggests that this pathway may also be important for other biological processes such as inflammation in which involvement of these two proteins has been shown (29, 30).

Results

Different Behavioral Outcomes from VAL 10 and VAL 25 Treatments with a Comparable Inhibitory Effect on GSK3β. To investigate potential dose-dependent effects of sodium valproate on GSK3β activity and behavior, mice were treated for 21 d with two different doses of sodium valproate: VAL 10 (10 g of sodium valproate per 1 kg of chow) or VAL 25 (25 g of sodium valproate per 1 kg of chow). Impact of treatment regimens on GSK3β (Ser-9) phosphorylation/inactivation was evaluated in the frontal cortex and striatum of mice treated with VAL 10 or VAL 25 or vehicle (normal chow). These two brain areas were chosen on the base of their known association with specific effects of GSK3β on locomotion in the case of the striatum and on mood/emotion-related responses in the case of the frontal cortex (24, 31). Both the VAL 10 and VAL 25 treatments resulted in an increased phosphorylation/inactivation of GSK3β compared with vehicle (Fig. 1*A*). Quantification of GSK3β and its negative regulator AKT using near infrared immunoblot analysis showed that the effect of both valproate treatment regimens on the phosphorylation of these proteins was comparable in the striatum and frontal cortex (Fig. 1 *B* and *C*). Previous study has shown that mice lacking βARR2 do not display changes in GSK3β activity following chronic lithium treatment (8). This suggests that these mice may provide a useful negative control model for the investigation of GSK3β regulation by mood stabilizers. Indeed, both valproate treatment

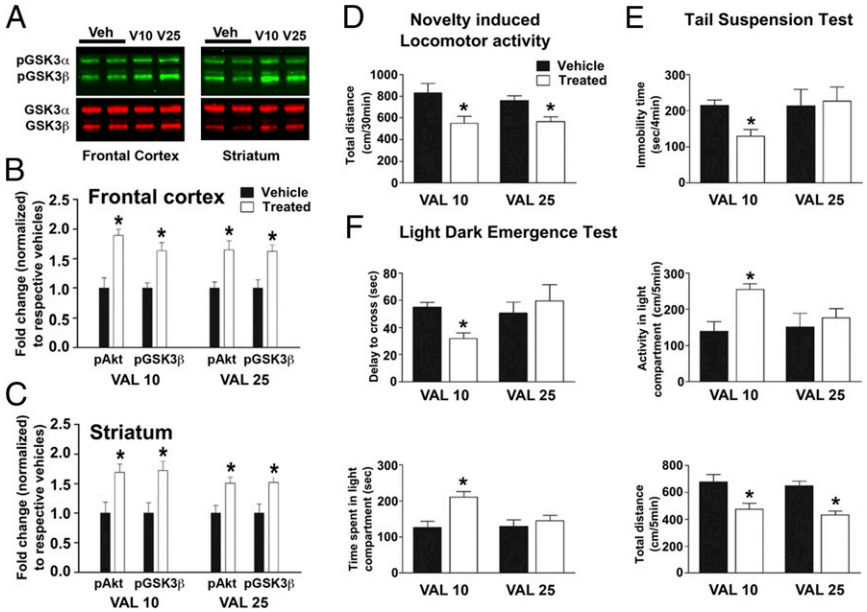

Fig. 1. Distinct behavioral outcomes despite comparable GSK3β inhibition following chronic treatments with different doses of valproate. (*A*) Immunoblot analysis of GSK3β phosphorylation in frontal cortex and striatum following VAL 10 and VAL 25 treatment. (*B* and *C*) Quantification of pAKT (Th308) and pGSK3β (Ser-9) levels in extracts prepared from the frontal cortex (*B*) or striatum (*C*) following chronic VAL 10 or VAL 25 treatment. (*D*) Locomotor activity in a novel environment for WT C57Bl6J mice treated chronically with valproate at two different doses: (VAL 10) 10 g or (VAL 25) 25 g of sodium valproate per 1 kg of chow for 21 d. Locomotion was measured as total distance traveled for the duration of the test (30 min). (*E*) TST for mice treated chronically with valproate at both doses. Behavior was scored as time spent in immobility (s) for the last 4 min of the test. (*F*) DLET for mice treated chronically with valproate at both doses. Behavior was scored as latency to first cross to the illuminated (light) compartment, time spent in the light compartment, activity in the illuminated (light) compartment, and total distance traveled in both compartments for the whole duration of the 5-min test. Data are means ± SEM. $^{*}P \leq 0.05$, $^{**}P \leq 0.01$, $^{***}P \leq 0.005$. For behavioral studies, one-way ANOVA with Bonferroni-corrected pair-wise comparisons was performed; $n = 10$ mice per group. For phosphorylation analysis, respective total protein signal was used as internal reference for phosphoproteins. Data were normalized to average protein levels in vehicle-treated animals. $^{*}P \leq 0.05$. Student double-tailed *t* test was performed (drug vs. vehicle within each genotype). $n = 5$ mice per group. Detection and quantification of immunoblot signal were performed within a linear signal range using near-infrared fluorescence and a LiCor Odyssey.

regimens failed to affect AKT and GSK3β phosphorylation in βARR2-KO mice (Fig. S1).

Mice were submitted to a series of behavioral tests that are responsive to lithium and selective GSK3β inhibition (8, 24). When tested, mice receiving either of the valproate treatment regimens displayed a reduction of exploratory behavior (Fig. 1*D*) that is similar to what is reported in mice treated with lithium or selective GSK3 inhibitors. In contrast, only mice treated under the VAL 10 conditions displayed a behavioral response in the TST (Fig. 1*E*). This lack of response to the VAL 25 treatment was also observed in the DLET (Fig. 1*F*). However, both treatment regimens reduced locomotion equally in this test, thus supporting that the lack of effects of the VAL 25 treatment on emotional dimensions of behavior in the DLET is not related to a greater reduction of locomotor activity.

Taken together, these observations indicate that, like it was reported for lithium (8), chronic valproate treatments can exert several behavioral effects by inhibiting GSK3β. However, these effects are different between the VAL 10 and VAL 25 conditions, suggesting that high doses of valproate may recruit additional mechanisms that could interfere with the behavioral outcomes of GSK3β inhibition.

Behavioral Effects of VAL 10 Treatment Correlate with Increased FXR1P Levels. A combination of VAL 10 and VAL 25 treatment regimens in WT and βARR2-KO mice was used as a model system to examine whether putative GSK3β substrates are affected differentially by treatments having different behavioral effects. In addition to valproate treatments, two pharmacological agents—lithium and lamotrigine—that are known to increase brain GSK3β phosphorylation (8, 19) and exert behavioral responses in the TST and DLET (Fig. S2 *A* and *B*) were also included as positive controls.

To identify possible new substrates involved in the regulation of behavior by GSK3β, we perused a list of putative priming-dependent GSK3β substrates established as part of a proteomic screen aimed at identifying proteins that can be targeted for degradation following phosphorylation by GSK3β (32). To maximize the chances of identifying a substrate with relevance to mental illnesses, this list was examined in light of existing literature on genetic loci associated to mental illness (28). Among the possible candidates, FXR1P, a RNA binding protein related to FMRP (27), was retained for further investigation.

The VAL 10 treatment as well as chronic treatment with lithium (15 d at a concentration of 0.12% wt/vol) or lamotrigine (21 d, 10 mg/kg, i.p.) all resulted in a robust up-regulation of FXR1P levels in the striatum and frontal cortex of mice (Fig. 2*A* and Fig. S2 *C–E*). Nevertheless, this up-regulation of FXR1P was absent in mice treated with the VAL 25 regimen or in βARR2-KO mice treated either with lithium, lamotrigine, or valproate (Fig. 2 *A* and *B* Fig. S2 *D–F*). Because antibodies directed against fragile X family proteins are known to display some levels of cross-reactivity, results obtained with the commercial antibody were further confirmed using an additional anti-FXR1P ML-12 antibody (33). Staining of the membranes with this antibody in Western blot (Fig. S2*C*) confirmed the selective increase of FXR1P levels in response to the VAL 10 treatment. Notably, in addition to the full-length 70-kDa isoforms of FXR1P, this antibody also detected an up-regulation of a 50-kDa band that may correspond to a degradation product of this protein (30).

Conditional GSK3β flox mice, lacking GSK3β expression in forebrain neurons as a result of a CamKII-driven Cre expression (24), were used to establish the potential contribution of an inhibition of GSK3β to this effect. As illustrated (Fig. 2*C*), neuronal GSK3β deficiency was accompanied by an increase in FXR1P levels in the frontal cortex of these mice compared with their Cre-negative littermates.

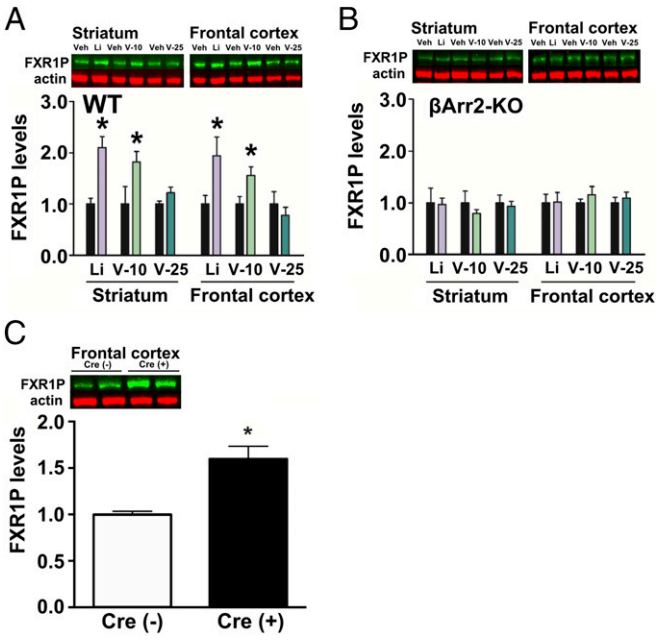

Fig. 2. Levels of FXR1P are regulated differentially by the VAL 10 and VAL 25 chronic treatments in vivo. (*A* and *B*) Quantitative immunoblot analysis of FXR1P levels in the striatum and the frontal cortex of (*A*) WT or (*B*) βARR2-KO mice treated chronically with lithium (LiCl, 0.12% in water), VAL 10, or VAL 25. (*C*) Quantitative immunoblot analysis of FXR1P levels in the frontal cortex of CamKII-Cre/GSK3β-Flox mice. Black bars in *A–C* correspond to control vehicle conditions. For all analyses, respective total protein signal was used as the internal reference for phosphoproteins. Data (means ± SEM) were normalized to average protein levels in vehicle-treated animals from the same genotype. $*P \leq 0.05$. Student double-tailed *t* test was performed (drug vs. vehicle within each genotype). $n = 5$ mice per group. Detection and quantification of immunoblot signal were performed within a linear signal range using near-infrared fluorescence and a LiCor Odyssey.

High-Dose Chronic Valproate Treatment Elicits Inhibition of ERK2. Because behavioral differences observed between the VAL 10 and VAL 25 treatment cannot be explained by a lack of GSK3β inhibition, we have explored the effects of sodium valproate on different major signaling pathways that may affect its regulation by GSK3β.

We used acute administrations to identify signaling pathways that may be affected by a high dose (400 mg/kg i.p.) of sodium valproate. Examination of striatal protein phosphorylation by Western blot at different times postinjection revealed (Fig. 3*A*) that this treatment caused a reduction of ERK2 phosphorylation 2 h after drug injection without affecting the phosphorylation of DARPP-32, CREB, or JNK. Further characterization of this effect using protein extracts obtained from the striatum or frontal cortex of mice treated with different doses (200, 300, or 400 mg/kg i.p.) of sodium valproate (Fig. 3*A*) showed that reduced ERK2 phosphorylation/activity occurred in both structures but was only significant at a 400 mg/kg dose, suggesting that this effect could be associated with the detrimental impact of high-dose valproate on behavioral responses.

To further examine this possibility, ERK2 phosphorylation was assessed in mice following VAL 10 and VAL 25 treatments (Fig. 3*B*). Although VAL 10 did not affect ERK2 phosphorylation, the VAL 25 treatment resulted in a reduction of ERK2 phosphorylation in both the cortex and striatum. Furthermore, this effect of VAL 25 on ERK2 phosphorylation did not occur in βARR2-KO mice (Fig. 3*C*). Because βARR2 has been implicated in the regulation of ERK2 activity by several G protein coupled receptors (GPCR) (34), this suggests that disruption of βARR2-mediated signaling by

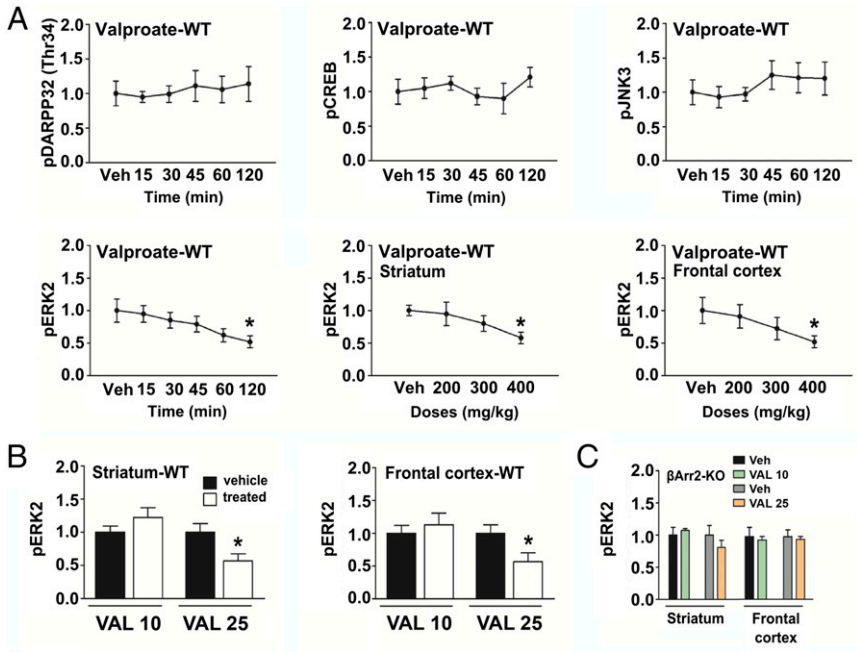

Fig. 3. High doses of valproate modulate ERK2 activity through a βARR2-dependent mechanism. (*A*) Quantitative immunoblot analysis of phosphoprotein levels of DARPP32, CREB, JNK3, and ERK2 proteins in the striatum of C57Bl6J WT mice at different times following acute treatment with valproate (sodium valproate, 400 mg/kg i.p.), and dose–response inhibition of ERK2 phosphorylation/activity by valproate as measured by quantitative immunoblot analysis 120 min after drug injection. (*B*) Quantitative immunoblot analysis of pERK2 levels in the striatum and frontal cortex of WT mice after VAL 10 or VAL 25 chronic valproate treatment or vehicle. (*C*) Quantitative immunoblot analysis of pERK2 levels in the striatum and frontal cortex of βARR2-KO after VAL 10 or VAL 25 chronic valproate treatment or vehicle. For all analyses, respective total protein signal was used as the internal reference for phosphoproteins. Data (means ± SEM) were normalized to average protein levels in vehicle-treated animals from the same genotype. $*P \leq 0.05$. Student double-tailed *t* test was performed (drug vs. vehicle within each genotype). $n = 5$ mice per group. Detection and quantification of immunoblot signal were performed within a linear signal range using near-infrared fluorescence and a LiCor Odyssey.

valproate in vivo is not restricted to mechanisms involving AKT and GSK3β. Interestingly, valproate has recently been shown to inhibit βARR2-mediated ERK2 activation downstream of the melatonin receptor type 1 in transfected HEK293 and Neuro2A cells (35), therefore supporting our findings in vivo.

To evaluate if a cross-talk between GSK3β and ERK2 can affect the regulation of behavior by GSK3β, we then tested how coadministration of the ERK2 kinase MEK inhibitor SL327 (50 mg/kg i.p.) affects behavioral responses to lithium (LiCl 75 mg/kg) or to the selective GSK3 inhibitor TDZD-8 (30 mg/kg i.p.). These doses of lithium and TDZD-8 were selected based on their known effects in mice (8). The dose of SL327 was selected to induce a level of ERK2 inhibition similar to the one resulting from the VAL 25 treatment in the mouse frontal cortex (Fig. S3 *A* and *B*). As it may be expected, both lithium and TDZD-8 induced an antidepressant-like response in the DLET when administered alone (Fig. S3*C*). However, this effect was fully abolished by coadministration of SL327.

Because valproate is a known inhibitor of class 1 histone deacetylase (HDAC1) (36), mice were treated with the HDAC1 inhibitor MS275 (20 mg/kg i.p. daily for 21 d) (37) to establish the impact of HDAC1 inhibition on FXR1P levels as well as ERK2, AKT, and GSK3β phosphorylation. Interestingly, MS275 treatment in WT animals did not affect FXR1P levels (Fig. S4*A*) or the phosphorylation of AKT, GSK3β, and ERK2 (Fig. S4*B*). However, this same treatment exerted an antidepressant-like effect in the TST in both WT and βARR2-KO mice (Fig. S4*C*). This suggests that like lithium, valproate regulates the activity of AKT and GSK3β and ERK2 via a βARR2-dependent mechanism that is independent from its effect on HDAC1 in vivo.

Regulation of the FXR1P Levels by GSK3β and ERK. A stable HEK293 cell line expressing a His-Tag recombinant mouse FXR1P under the control of a CMV promoter was generated to study the effects of ERK2 and GSK3β activity on FXR1P levels directly. Treatment of cells with GSK3 inhibitors TDZD-8, lithium, SB216763, and alsterpaullone resulted in an increase of the levels of the recombinant FXR1P (Fig. 4*A*). Furthermore, expression of a constitutively active AKT resulted in an increase in the inhibitory phosphorylation of GSK3β accompanied by increased levels of recombinant FXR1P (Fig. S5*A*). Conversely, expression of a constitutively active S9A mutant of GSK3β led to reductions of the recombinant FXR1P (Fig. S5*B*) that was prevented by TDZD-8 (Fig. S5*C*). Finally, although inhibition of ERK2 phosphorylation/activation by SL327 had no effect on the levels of recombinant FXR1P (Fig. 4*B*), cotreatment with SL327 abolished the effects of TDZD-8 on recombinant FXR1P level without preventing the increase of endogenous β-catenin resulting from GSK3β inhibition (Fig. 4*C*). β-catenin is a constituent of the Wnt pathway that is degraded by the ubiquitin proteasome system following its phosphorylation (38). Taken together experiments conducted using the recombinant cell line suggest that GSK3β negatively regulates the FXR1P, potentially by targeting it for degradation, as it does for β-catenin. However, in contrast to the action of GSK3β on β-catenin, the action of this kinase is dependent upon a tonic activation of ERK2, therefore suggesting priming of FXR1P by ERK2 as a potential mechanism.

ERK2 Activity Favors FXR1P Phosphorylation and Regulation by GSK3β. Examination of the FXR1P sequence (Fig. 4*D*) revealed the existence of nine putative GSK3β consensus sites localized in the carboxyl-terminal portion of the protein between amino acids 400 and 570. Interestingly, most of these sites are situated in a region of FXR1P that shows less than 6% homology with other proteins of the fragile X mental retardation family (27). In vitro phosphorylation assays were carried out to establish whether FXR1P is

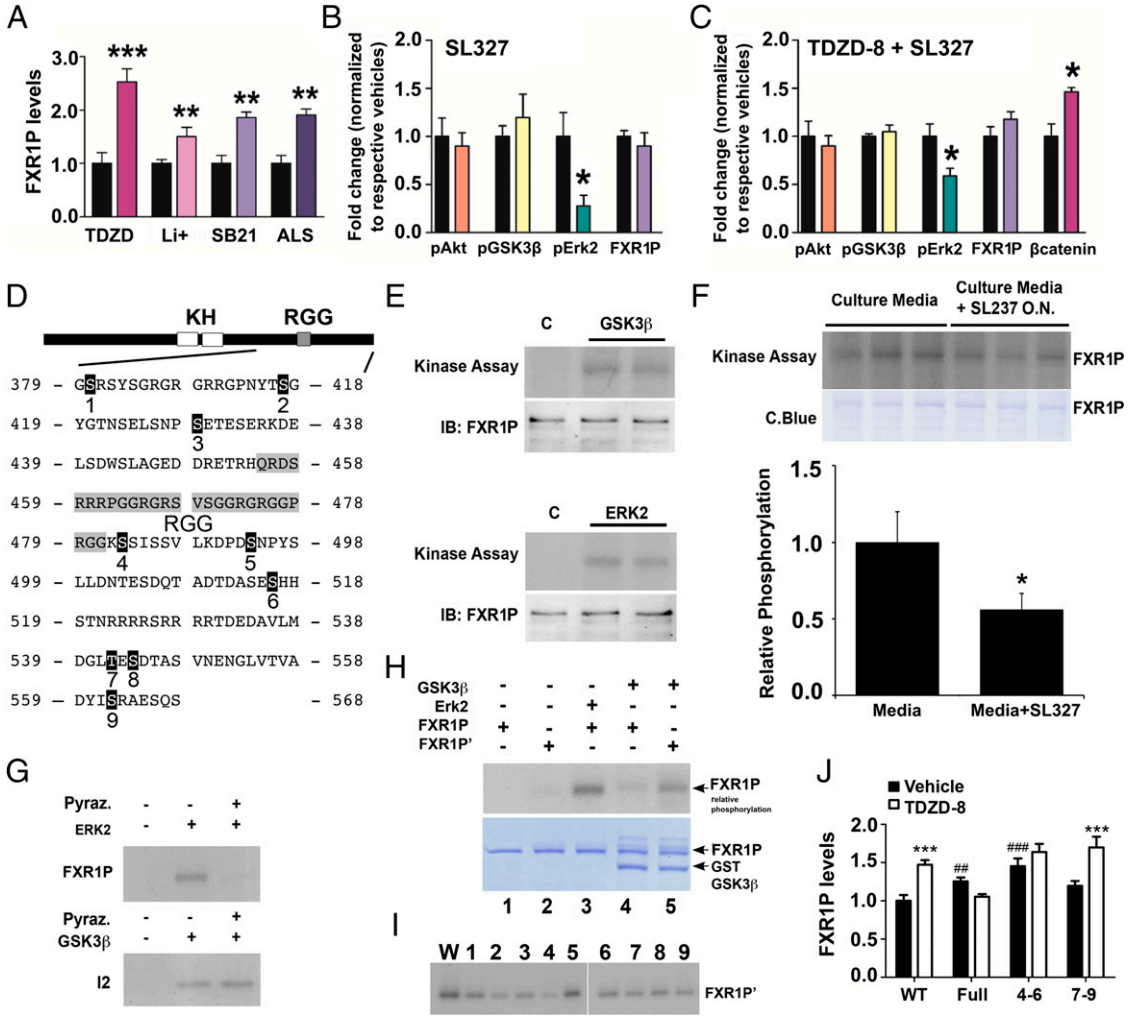

Fig. 4. Regulation of FXR1P by GSK3β and ERK signaling. (*A–C*) Quantitative immunoblot analysis of protein and/or phosphoprotein levels in stably transfected HEK293 cells expressing his-tagged recombinant mouse FXR1P. (*A*) FXR1P levels 60 min following treatments with TDZD-8 (10 μM), lithium (2 mM), SB216763 (10 μM), and alsterpaulone (10 μM). (*B*) Cells were treated with SL327 (10 μM, 60 min) or (*C*) with TDZD-8 and SL327. Black bars correspond to control vehicle conditions. Respective total protein signal was used as the internal reference for phosphoproteins. Actin was used as a reference for the measurement of changes in the relative levels of a given protein. Data (means ± SEM) were normalized to average protein levels in vehicle-treated cells. $*P \leq 0.05$, $**P \leq 0.01$, $***P \leq 0.005$. Student double-tailed *t* test was performed (drug vs. vehicle within each genotype). $n = 5$ separate cell cultures. Detection and quantification of immunoblot signal were performed within a linear signal range using near-infrared fluorescence and a LiCor Odyssey. (*D*) Identification of putative GSK3β phosphorylation sites within the His-FXR1P sequence. Individual serine and threonine (in black) are numbered. KH and RGG domains are indicated. (*E*) In vitro phosphorylation of recombinant HEK293 cell produced his-tagged FXR1P with radioactive ATP by recombinant GSK3β or ERK2. (*F*) Quantitative assessment of in vitro phosphorylation by recombinant GSK3β of recombinant his-tagged FXR1P produced in HEK293 cells that were incubated overnight with media containing SL327 (10 μM) or vehicle. Kinase assays were performed in parallel. Each lane corresponds to kinase assays made from different immunoprecipitates. Absorbance of the Coomassie blue (C. blue)-stained FXR1P band of corresponding immunoprecipitates was used as a control for variation of FXR1P abundance between immunoprecipitates. Data are means ± SEM; $n = 3$; $*P \leq 0.05$ (Student double-tailed *t* test). (*G*) Effect of the ERK inhibitor pyraz (1 μM) on the phosphorylation by recombinant ERK2 of recombinant his-tagged FXR1P produced in *E. coli* (*Top*) and of the GSK3 substrate inhibitor 2 (I2) by recombinant GSK3β (*Bottom*). (*H*) Effect of a prior phosphorylation by ERK2 on the phosphorylation of *E. coli* produced his-tagged FXR1P by GSK3β in the presence of [γ^{32}P]ATP. Recombinant his-tagged FXR1P was incubated with recombinant ERK2 and nonradioactive ATP to produce an ERK2 primed form of FXR1P (FXR1P′). This reaction was then stopped by addition of pyraz. FXR1P and FXR1P′ were used for phosphorylation assays in the presence of radioactive ATP. Additional bands in lanes 4 and 5 of the Coomassie blue-stained gel correspond to the human GST-GSK3β recombinant protein that was used in the assay. Gel presented is representative of five independent experiments. (*I*) In vitro phosphorylation assays of individual serine-threonine to alanine mutants of his-tagged FXR1P′ produced in *E. coli*. All mutants were primed with ERK2 before kinase assay. Gel presented is representative of five independent experiments. (*J*) Quantitative immunoblot analysis of HA-FXR1P and HA-FXR1P alanine mutants after 60 min of treatment with TDZD-8 in 293-HEK cells. $**P \leq 0.01$, $***P \leq 0.005$. One-way ANOVA with Bonferroni-corrected pair-wise comparisons was performed; $n = 5$ separate cell cultures.

phosphorylated by GSK3β and ERK2. In a first set of experiments, His-Tag recombinant mouse FXR1P was immunoprecipitated from the stable HEK293 cell line and used as a substrate for phosphorylation. As shown (Fig. 4*E*), incubation of the protein with radioactive [γ^{32}P]ATP and recombinant GSK3β or ERK2 resulted in its phosphorylation. Interestingly, overnight pretreatment of HEK293 cells with SL237 before recombinant mouse FXR1P immunoprecipitation resulted in a reduction in the level of FXR1P phosphorylation by recombinant GSK3β (Fig. 4*F*), therefore supporting the hypothesis that phosphorylation by ERK2 can facilitate the phosphorylation of FXR1P by GSK3β.

Because the phosphorylation of FXR1P by ERK2 cannot be fully inhibited in mammalian cells, recombinant FXR1P was produced in *Escherichia coli* to address the role of ERK2 in regulating

the phosphorylation of FXR1P by GSK3β. Incubation of bacterially produced recombinant FXR1P with ERK2 resulted in its phosphorylation (Fig. 4*G*). Importantly, this action of ERK2 was abolished by its selective inhibitor 3-Methyl-5-pyrazolone (pyraz). However, pyraz did not prevent the phosphorylation of the GSK3β substrate (39) protein phosphatase inhibitor 2 (I2) by GSK3β (Fig. 4*G*). This allowed for performing a phosphorylation of FXR1P by ERK2 in the presence of nonradioactive ATP to generate a primed recombinant FXR1P (FXR1P′) that was then treated with pyraz to inactivate ERK2 activity. Incubation of FXR1P or FXR1P′ with γP^{32}-labeled ATP in the absence of additional kinases did not result in the incorporation of radioactive phosphates in either recombinant proteins, therefore indicating that pyraz totally inhibited the activity of ERK2 used to generate FXR1P′ (Fig. 4*H*, lanes 1 and 2). Incubation of FXR1P with recombinant GSK3β resulted in a very low level of FXR1P phosphorylation (Fig. 4*H*, lane 4). In contrast prephosphorylation of FXR1P by ERK2 allowed for a much greater level of phosphorylation of FXR1P′ by GSK3β (Fig. 4*H*, lane 5), thus confirming that, at least in vitro, ERK2 phosphorylation facilitates phosphorylation of FXR1P by GSK3β.

To try identifying the site responsible for the phosphorylation of FXR1P′ by GSK3β, individual putative serine or threonine phosphorylation sites were mutated to alanine, and the nine different his-tagged recombinant mutants of FXR1P were produced in *E. coli*. Kinase assays were carried out on primed versions of these proteins. Although all mutations somewhat reduced the phosphorylation of FXR1P′ by GSK3β, no individual mutation was sufficient to fully abolish phosphorylation (Fig. 4*I*), suggesting that multiple functional GSK3β sites are present in the carboxyl-terminal domain of FXR1P.

HA-tagged WT and mutant versions of FXR1P were generated. In a "full" mutant, all putative GSK3β phosphorylatable residues were mutated to alanine. Two partial mutants where only putative sites 4–6 or 7–9 (Fig. 4*D*) were mutated to alanines were also made. Vectors encoding WT-HA-FXR1P or the different mutants were transiently transfected to HEK293 cells, and the impact of inhibition of GSK3 by TDZD-8 on HA-FXR1P levels was quantified by near-infrared immunoblot analysis (Fig. 4*J*). The abundance of the WT-HA-FXR1P was elevated following treatment with TDZD-8. Furthermore, levels of the mutant lacking the putative phosphorylation sites 7–9 were also increased. In contrast, both the full mutant FXR1P and the mutant lacking sites 4, 5, and 6 were resistant to TDZD-8 treatment. Interestingly, basal levels of the full and 4–6 mutants were also elevated under control conditions compared with WT-HA-FXR1P. Taken together, these observations suggest that phosphorylation of FXR1P on sites 4, 5, and/or 6 is one of the factors contributing to the regulation of FXR1P by GSK3β.

FXR1P Overexpression Replicates Behavioral Effects of Valproate and GSK3β Inhibition. The potential contribution of FXR1P to the effects resulting from the VAL 10 treatment and GSK3β inhibition was evaluated using an adeno-associated viral (AAV) vector overexpressing a recombinant GFP-FXR1P. Previous results obtained from CamKII-Cre/GSK3β flox mice have shown that inactivation of forebrain GSK3β is sufficient to induce responses in the DLET, while having no effect in the TST (24). To further validate this site of intervention, the GSK3β gene was inactivated (Fig. S6*A*) in the prefrontal cortex of GSK3β flox mice using an AAV vector expressing a GFP-Cre fusion protein (40). Evaluation of these mice in the DLET 3 wk after infection confirmed that inactivation of GSK3β in this brain area is sufficient to induce behavioral responses in this test (Fig. S6*B*).

An AAV vector driving the expression of GFP-FXR1P in neurons under the control of a synapsin promoter was then used to assess behavioral consequences of FXR1P overexpression in this brain area (Fig. 5*A*). Evaluation of FXR1P levels 3 wk after infection showed a robust GFP-FXR1P expression in the prelimbic prefrontal cortex (Fig. 5*B*) compared with control mice infected with a AAV vector driving the expression of GFP under the control of the same synapsin promoter. Furthermore, histological examination confirmed the presence of recombinant GFP-FXR1P in the cell body and MAP2-positive dendrites of infected cortical neurons (Fig. 5*C*), thus confirming that the subcellular distribution of GFP-FXR1P corresponds to that of endogenous FXR1P (41). Finally, overexpression of GFP-FXR1P in prelymbic prefrontal cortex neurons replicated the behavioral effects of GSK3β deletion and VAL 10 treatment in the DLET (Fig. 5 *D–F*), indicating that an increase in FXR1P level is sufficient to exert effects similar to those of GSK3β inhibition on mood/emotion-related behaviors.

***FXR1* Gene Polymorphism rs496250 Is Associated with mRNA Expression in Postmortem Human Brain.** To support the biological interaction between GSK3β and FXR1P for phenotypes of relevance for mood regulation in humans, we explored if SNPs within genes encoding GSK3β and FXR1P (*GSK3B*, 3q13.3 and *FXR1*, 3q28, respectively) have functional interaction in modulating human brain activity and behavior related to emotion processing. In particular, we focused on *GSK3B* rs12630592 (G/T), for which the G allele has been associated with higher GSK3β expression (3). Furthermore, we investigated SNPs located in the promoter region of *FXR1* and characterized in the publicly available database of postmortem brains Braincloud (42). We identified two SNPs within the *FXR1* promoter region, rs1805562 (A/C) and rs496250 (A/G), occurring 1,052 bp and 3,148 bp upstream of the gene, respectively. Age, sex, pH, RNA integrity number, and postmortem interval were homogeneously distributed among genotype groups for both SNPs ($P > 0.05$).

An analysis of covariance (ANCOVA) with the rs1805562 genotype as predictor and age as well as the Age × Genotype interaction as covariates of no interest did not reveal an effect of this genotype on *FXR1* mRNA expression [$F_{(1,90)} = 0.0006$; $P > 0.9$]. In contrast, a similar analysis indicated a main effect of rs496250 on the same dependent variable. In particular, subjects carrying the A allele of this SNP had higher levels of FXR1P mRNA compared with subjects homozygous for the G allele [$F_{(1,90)} = 6.40$; $P = 0.013$] (Fig. S7*A*).

Thus, we used rs496250 and rs12630592 as proxies of *FXR1* and *GSK3B* gene expression level to be used in further analyses addressing the interaction between *GSK3B* and *FXR1* variation on phenotypes related to emotion processing in healthy humans.

Interaction Between *GSK3B* and *FXR1* Predicts Amygdala Activity During Processing of Facial Expressions. We investigated if the interaction between genetic variation within *GSK3B* and *FXR1* affecting gene expression has functional effects on imaging phenotypes linked to physiological aspects of emotion processing. With this aim, we tested in healthy humans if *GSK3B* rs12630592 and *FXR1* rs496250 have a combined effect on amygdala response while subjects implicitly evaluated facial expressions during fMRI. ANOVAs and χ^2 tests indicated that *GSK3B*/*FXR1* genotype groups did not differ in terms of age, IQ, socioeconomic status, handedness, and behavioral performance at the fMRI task (all $P > 0.1$), whereas sex was unequally distributed between groups ($\chi^2 = 5.54$; $P = 0.02$). Statistical parametric mapping ANCOVA with sex as a covariate of no interest indicated a main effect of facial expression in the left amygdala ($x = -26$, $y = 4$, $z = -18$; K = 122; Z = 5.47; FWE-$P < 0.001$), whereas there was no effect of *FXR1* or of *GSK3B* variation in this brain region during processing of facial expressions. However, there was an interaction between *FXR1* rs496250 and *GSK3B* rs12630592 in left amygdala activity ($x = -20$, $y = -2$, $z = -18$; K = 30; Z = 3.20; FWE-$P = 0.026$) (Fig. 5 *G* and *H*). Analysis of BOLD response extracted from this significant cluster revealed that amygdala activity was modulated by *GSK3B* rs12630592 only in the context of *FXR1* rs496250 A carriers. In particular, *FXR1*

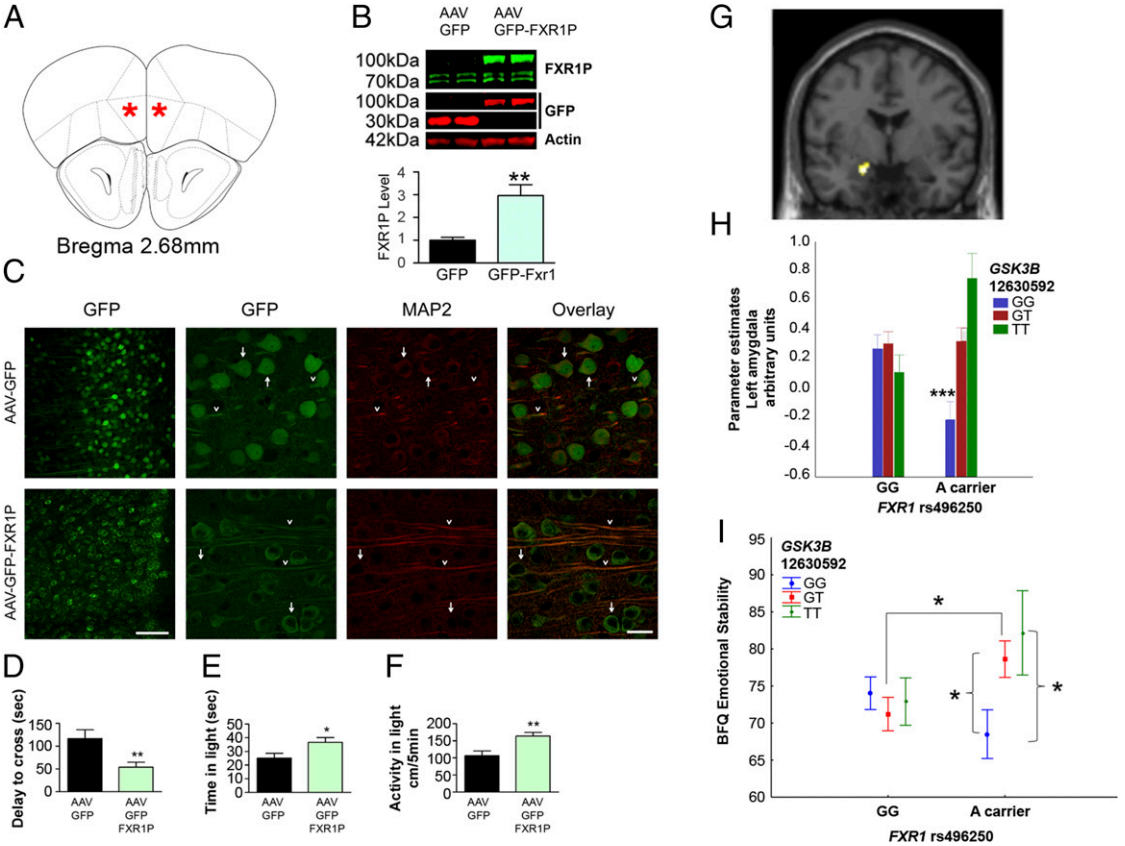

Fig. 5. FXR1P regulates mood and emotion-related responses in mice and humans. (*A*) Representation of the area targeted for injections of AAV expression vectors (adapted from ref. 58). (*B*) Quantitative immunoblot analysis of FXR1P and GFP-FXR1P levels in the frontal cortex 3 wk following infection with either AAV-GFP-FXR1P or AAV-GFP vectors. Actin was used as a reference for the measurement of changes in the relative levels of total FXR1P (endogenous + GFP-FXR1P). Data (means ± SEM) were normalized to average protein levels in AAVmKate-infected animals from the same genotype. $*P \leq 0.05$ (Student double-tailed *t* test). $n = 10$ animals per group. (*C*) Fluorescence microscopy imaging of the frontal cortex of a mouse infected with the GFP or GFP-FXR1P vectors, indicating that the synapsin promoter used in the vector targets fluorescent transgene protein expression to cells having a neuronal morphology and showing distribution of GFP and GFP-FXR1P in neuronal cell bodies (arrow) and MAP2-positive dendrites (arrowhead). [Scale bar, (two left-hand panels) 100 μm and (all other panels) 25 μm.] (*D–F*) DLET mice injected either with the GFP-FXR1P or GFP vectors. Behavior was scored as (*D*) latency to first cross to the illuminated (light) compartment, (*E*) time spent in the light compartment, and (*F*) activity in the illuminated (light) compartment for the whole duration of the 5-min test. Data are means ± SEM. $*P \leq 0.05$, $**P \leq 0.01$. One-way ANOVA with Bonferroni-corrected pair-wise comparisons was performed; $n = 10$ mice per group. (*G*) Coronal section of the brain showing the cluster in the left amygdala associated with a *FXR1* rs496250 by *GSK3B* rs12630592 interaction. (*H*) Parameter estimates extracted from the significant cluster. *GSK3B* GG individuals have lower activity in the left amygdala compared with *GSK3B* GT and *GSK3B* TT subjects only in the context of *FXR1* A carrier genotype. Data are means ± SEM; $***P \leq 0.001$; see text for details of statistical analysis. (*I*) Interaction between *FXR1* rs496250 and *GSK3B* rs12630592 on emotional stability dimension of the BFQ. Data are means ± SEM; $*P \leq 0.05$; details of statistical analysis are described in *Results*.

rs496250 A carrier/*GSK3B* GG individuals had lower amygdala activity compared with *FXR1* rs496250 A carrier/*GSK3B* TT ($P < 0.001$) and *FXR1* rs496250 A carrier/*GSK3B* GT ($P < 0.001$) subjects. Furthermore, the latter group had lower amygdala activity than *FXR1* rs496250 A carrier/*GSK3B* TT ($P = 0.017$) individuals. No modulation of amygdala activity by *GSK3B* rs12630592 was present in the context of *FXR1* rs496250 GG genotype.

Interaction Between *GSK3B* and *FXR1* Predicts Scores of "Emotional Stability" Within the BFQ. To investigate if *GSK3B* rs12630592 and *FXR1* rs496250 also interact in modulating behavioral correlates of emotion processing in healthy individuals, we used the Big Five Questionnaire (BQF), which measures five aspects of personality including emotional stability (43). In particular, individuals with low scores on emotional stability often report emotional instability and negative emotions such as anxiety, depression, or anger. Thus, we used emotional stability as the dimension of interest for our analysis. Genotype groups were matched for age, sex, full-scale IQ, and parental socioeconomical status (all *P*s > 0.1). Factorial ANOVA indicated no main effects of *GSK3B* rs12630592 [$F_{(2,147)} = 1.69$, $P > 0.1$] and of *FXR1* rs496250 [$F_{(1,147)} = 1.79$, $P > 0.1$) on emotional stability. However, there was a genotype/genotype interaction on this measure [$F_{(2,147)} = 3.66$, $P = 0.028$]. Post hoc analysis revealed that in the context of low (*GSK3B* rs12630592 TT) to medium (*GSK3B* rs12630592 GT) *GSK3B* expression, *FXR1* A carrier displayed higher emotional stability (Fig. 5*I*). However, *FXR1* A carriers/*GSK3B* GG subjects—that have higher *GSK3B* expression—had lower scores than *FXR1* A carriers/*GSK3B* GT and *FXR1* A carriers/*GSK3B* TT individuals (Fig. 5*I*). No significant effect of *GSK3B* rs12630592 was present in the context of *FXR1* rs496250 GG genotype. Furthermore, other dimensions of the BQF were not affected by *FXR1*/*GSK3B* interactions (Fig. S7*B*). These data support that increased expression of the GSK3β substrate FXR1P has a positive action on emotional stability in humans. Genetic interaction between *FXR1* and *GSK3B* also supports a negative role for GSK3β in the regulation of FXR1P that is compatible with our observations in mice and in vitro systems.

Discussion

Results presented here identify FXR1P as a substrate of GSK3β involved in the regulation of mood and emotional control. Our

findings in animals indicate that inhibition of neuronal GSK3β either in GSK3β flox mice or following chronic treatment with valproate, lamotrigine, or lithium results in an increase of FXR1P levels that coincides with the mood-related effects of these drugs and of GSK3β inhibition. Overexpression of FXR1P in the mouse prefrontal cortex elicits relevant behavioral responses even in βARR2-KO mice, which are generally resistant to the behavioral effects of mood stabilizers. Consistently, results in humans indicate that the genetic interaction of functional variations in *FXR1* and *GSK3B* is associated with activity of the amygdala, a brain area involved in emotion processing that is innervated and regulated by the prefrontal cortex (44, 45). Furthermore, *FXR1*/*GSK3B* interaction affects emotional behavior in healthy subjects in whom higher *FXR1* expression is associated to greater emotional stability, except in the context of higher *GSK3B* expression. Together, these results suggest that the interplay between FXR1P and GSK3β is crucial in determining patterns of physiological and behavioral responses relevant to the modulation of emotional responses implicated in mood.

Our results in recombinant systems suggest that phosphorylation of one or several putative GSK3β sites is involved in regulating FXR1P levels, possibly by enhancing its degradation. However, whether this is the only way this regulation occurs in vivo and the precise nature of its mechanism will need to be characterized further. Additionally, GSK3α activity is also regulated in response to lithium (46) and other mood stabilizers. Because the two isoforms of GSK3 share several substrates (2), it is possible that GSK3α may contribute to the regulation of FXR1P. Our results also indicate that valproate can interfere with at least two modalities of βARR2-mediated signaling, the negative regulation of AKT and the activation of ERK2. Interestingly, a similar effect of valproate has recently been reported in neuroblastoma cells (35). However, this effect does not seem to be apparent at all doses, as only the VAL 25 regimen resulted in a βARR2-dependent reduction of ERK activity in vivo. It is thus possible that the mechanisms of this interference may vary across signaling complexes downstream of different cell surface receptors. Characterization of these mechanisms represents another attractive topic for future investigations streaming from our observations.

FXR1P is an RNA binding protein that belongs to the same family as FXR2 and FMRP. Proteins from this family have been mostly studied in the context of the fragile X mental retardation syndrome and autism spectrum disorders. Observation of a contribution of FXR1P to the regulation of mood and emotions suggests that the role of this family of proteins could be extended to other types of mental illnesses. FXR1P contains two KH domains and a RGG box that are implicated in mediating its interactions with mRNAs as well as with other proteins (47). Although FMRP and to a lesser extent FXR2 have been extensively studied, little is known about the functions of FXR1P in the brain. One major limitation for such studies is that FXR1P gene knockout mice die shortly after birth due to a deficit in muscle formation (48).

A study of hippocampal neurons has shown an association of FXR1P with neuronal polyribosomes in dendritic clusters (41). Furthermore, FXR1P has been recently identified as a negative regulator for the translation of the ionotopic-glutamate AMPA receptor subunit GluA2. As a consequence of this, FXR1P would act as an inhibitor of protein synthesis-dependent long-term potentiation (49). In this context, it is possible that by increasing FXR1P, GSK3β inhibition can act as a buffer by limiting synaptic plasticity. Interestingly, this consequence of GSK3β inhibition would be compatible with its putative involvement in mood stabilization.

In addition, FXR1P is also a known translational regulator of the tumor necrosis factor alpha (TNFα), a key cytokine involved in tumorigenesis and inflammation. Binding of FXR1P to the 3′ untranslated region of the TNFα mRNA in macrophages has been shown to inhibit its translation (50). However, cross-regulation of this same mRNA by FXR1P and Argonaute 2 results in the opposite effect (30). Interestingly, several lines of evidence suggest a role for inflammation and TNFα in mental illnesses including bipolar disorder and schizophrenia (51–53). Furthermore, evidence for an anti-inflammatory action of mood stabilizers and of more selective GSK3β inhibitors has been reported (29). It is therefore possible that FXR1P may exert its action on mood by regulating TNFα mRNA translation.

A large-scale association study identified *FXR1* as a genetic risk factor for schizophrenia (28). However, beyond genome-wide association studies, the involvement of FXR1P in schizophrenia or other psychiatric illness is essentially unexplored. Our findings in mice and humans are suggestive of a role for the GSK3β/FXR1P pathway in regulating emotion processing and stability, behavioral dimensions involved in both schizophrenia and bipolar disorder. Furthermore, up-regulation of FXR1P is a shared consequence of behaviorally effective treatment with three major mood stabilizers, thus suggesting that it may contribute to the therapeutic action of these drugs. However, this will have to be firmly established by further research. Furthermore, our observations using MS275 in the TST also indicate that inhibition of HDAC1 activity may also contribute to the clinical actions of valproate independently of GSK3 and βARR2. Schizophrenia and bipolar disorder share several genetic risk factors (54, 55), and defective GSK3β signaling is a suspected contributing mechanism to both disorders. However, additional research will be needed to firmly support this role of the GSK3β/FXR1P signaling pathway and contemplate its use as a potential therapeutic opportunity. That being said, results presented here uncovered an unappreciated interaction between FXR1P and GSK3β with an involvement in regulating behavioral dimensions pertinent for mental illnesses.

Methods

Detailed experimental procedures are available in *SI Methods*. A list of primers used to generate the different FXR1P mutants is also provided in Table S1.

Experimental Animals. All experimental procedures were approved by the Université Laval Institutional Animal Care Committee according to guidelines from the Canadian Council on Animal Care. Sodium valproate (Sigma-Aldrich) was administered for a period of 21 d in chow at a concentration of 10 (VAL 10) or 25 (VAL 25) g per 1 kg of chow as described (56).

Quantitative Immunoblots. Euthanasia and immunoblot analyses were performed as described (21) and imaged in the near infrared using a Odyssey Imager (Licor Biotechnology).

Measurement of Locomotor Activity. Locomotion was evaluated under illuminated conditions in an automated Omnitech Digiscan apparatus (AccuScan Instruments) as described (21).

TST. Mice were tested for 6 min in a tail suspension apparatus (Med-Associates) as described (23, 57).

DLET. The DLET was performed as described (26, 57). Tests were conducted using an automated open field activity setup with light/dark insert (Med-Associates).

Human Subjects. All subjects included in the human study provided written informed consent to the study after the procedure was fully explained to them. The protocol was approved by the local Institutional Review Board. Detailed experimental groups and statistical methods are available in *SI Methods*.

ACKNOWLEDGMENTS. We thank Nathalie Bouchard and Kathye Aubé for assistance maintaining mouse colonies; Dr. Robert Lefkowitz and Dr. Marc G. Caron (Duke University Medical Center, Durham, NC) for βArrestin2-KO mice; and Dr. James Woodgett (Samuel Lunefeld Research Institute, Toronto, Canada) for GSK3β-Fl mice and vectors expressing activated GSK3β and AKT. We also thank Gohar Fakhfouri for careful proofreading of the manuscript. This work was supported by a Canadian Institute of Health Research operating

grant (to J.-M.B.) and from Fondazione con il sud (to A.R.). M.L. was supported by a postdoctoral fellowship from the Fond de Recherche du Québec en Santé. J.-M.B. holds a Canada Research Chair in Molecular Psychiatry and is an International Mental Health Organization Rising Star Awardee.

1. Embi N, Rylatt DB, Cohen P (1980) Glycogen synthase kinase-3 from rabbit skeletal muscle. Separation from cyclic-AMP-dependent protein kinase and phosphorylase kinase. *Eur J Biochem* 107(2):519–527.
2. Kaidanovich-Beilin O, Woodgett JR (2011) GSK-3: Functional insights from cell biology and animal models. *Front Mol Neurosci* 4:40.
3. Blasi G, et al. (2013) Association of GSK-3β genetic variation with GSK-3β expression, prefrontal cortical thickness, prefrontal physiology, and schizophrenia. *Am J Psychiatry* 170(8):868–876.
4. Network and Pathway Analysis Subgroup of Psychiatric Genomics Consortium (2015) Psychiatric genome-wide association study analyses implicate neuronal, immune and histone pathways. *Nat Neurosci* 18(2):199–209.
5. Klein PS, Melton DA (1996) A molecular mechanism for the effect of lithium on development. *Proc Natl Acad Sci USA* 93(16):8455–8459.
6. Emamian ES, Hall D, Birnbaum MJ, Karayiorgou M, Gogos JA (2004) Convergent evidence for impaired AKT1-GSK3beta signaling in schizophrenia. *Nat Genet* 36(2): 131–137.
7. Alimohamad H, Rajakumar N, Seah YH, Rushlow W (2005) Antipsychotics alter the protein expression levels of beta-catenin and GSK-3 in the rat medial prefrontal cortex and striatum. *Biol Psychiatry* 57(5):533–542.
8. Beaulieu JM, et al. (2008) A beta-arrestin 2 signaling complex mediates lithium action on behavior. *Cell* 132(1):125–136.
9. Li X, et al. (2004) In vivo regulation of glycogen synthase kinase-3beta (GSK3beta) by serotonergic activity in mouse brain. *Neuropsychopharmacology* 29(8):1426–1431.
10. Kaidanovich-Beilin O, Milman A, Weizman A, Pick CG, Eldar-Finkelman H (2004) Rapid antidepressive-like activity of specific glycogen synthase kinase-3 inhibitor and its effect on beta-catenin in mouse hippocampus. *Biol Psychiatry* 55(8):781–784.
11. Beaulieu JM, Gainetdinov RR, Caron MG (2009) Akt/GSK3 signaling in the action of psychotropic drugs. *Annu Rev Pharmacol Toxicol* 49:327–347.
12. Duman RS (2014) Neurobiology of stress, depression, and rapid acting antidepressants: Remodeling synaptic connections. *Depress Anxiety* 31(4):291–296.
13. Martinez A (2006) TDZD: Selective GSK-3 inhibitor with great potential for Alzheimer disease. *Neurobiol Aging* 27(S1):S13.
14. Hall AP, Escott KJ, Sanganee H, Hickling KC (2015) Preclinical toxicity of AZD7969: Effects of GSK3β inhibition in adult stem cells. *Toxicol Pathol* 43(3):384–399.
15. Chu B, Soncin F, Price BD, Stevenson MA, Calderwood SK (1996) Sequential phosphorylation by mitogen-activated protein kinase and glycogen synthase kinase 3 represses transcriptional activation by heat shock factor-1. *J Biol Chem* 271(48): 30847–30857.
16. Frame S, Cohen P (2001) GSK3 takes centre stage more than 20 years after its discovery. *Biochem J* 359(Pt 1):1–16.
17. Jope RS, Bijur GN (2002) Mood stabilizers, glycogen synthase kinase-3beta and cell survival. *Mol Psychiatry* 7(Suppl 1):S35–S45.
18. Li X, Bijur GN, Jope RS (2002) Glycogen synthase kinase-3beta, mood stabilizers, and neuroprotection. *Bipolar Disord* 4(2):137–144.
19. Abelaira HM, et al. (2011) Effects of acute and chronic treatment elicited by lamotrigine on behavior, energy metabolism, neurotrophins and signaling cascades in rats. *Neurochem Int* 59(8):1163–1174.
20. O'Brien WT, et al. (2011) Glycogen synthase kinase-3 is essential for β-arrestin-2 complex formation and lithium-sensitive behaviors in mice. *J Clin Invest* 121(9): 3756–3762.
21. Beaulieu JM, et al. (2004) Lithium antagonizes dopamine-dependent behaviors mediated by an AKT/glycogen synthase kinase 3 signaling cascade. *Proc Natl Acad Sci USA* 101(14):5099–5104.
22. Young JW, et al. (2010) GBR 12909 administration as a mouse model of bipolar disorder mania: Mimicking quantitative assessment of manic behavior. *Psychopharmacology (Berl)* 208(3):443–454.
23. Crowley JJ, Jones MD, O'Leary OF, Lucki I (2004) Automated tests for measuring the effects of antidepressants in mice. *Pharmacol Biochem Behav* 78(2):269–274.
24. Latapy C, Rioux V, Guitton MJ, Beaulieu JM (2012) Selective deletion of forebrain glycogen synthase kinase 3β reveals a central role in serotonin-sensitive anxiety and social behaviour. *Philos Trans R Soc Lond B Biol Sci* 367(1601):2460–2474.
25. Chakraborty A, Latapy C, Xu J, Snyder SH, Beaulieu JM (2014) Inositol hexakisphosphate kinase-1 regulates behavioral responses via GSK3 signaling pathways. *Mol Psychiatry* 19(3):284–293.
26. Weisstaub NV, et al. (2006) Cortical 5-HT2A receptor signaling modulates anxiety-like behaviors in mice. *Science* 313(5786):536–540.
27. Siomi MC, et al. (1995) FXR1, an autosomal homolog of the fragile X mental retardation gene. *EMBO J* 14(11):2401–2408.
28. Schizophrenia Working Group of the Psychiatric Genomics Consortium (2014) Biological insights from 108 schizophrenia-associated genetic loci. *Nature* 511(7510): 421–427.
29. Beurel E, Jope RS (2014) Inflammation and lithium: Clues to mechanisms contributing to suicide-linked traits. *Transl Psychiatry* 4:e488.
30. Vasudevan S, Steitz JA (2007) AU-rich-element-mediated upregulation of translation by FXR1 and Argonaute 2. *Cell* 128(6):1105–1118.
31. Urs NM, Snyder JC, Jacobsen JP, Peterson SM, Caron MG (2012) Deletion of GSK3β in D2R-expressing neurons reveals distinct roles for β-arrestin signaling in antipsychotic and lithium action. *Proc Natl Acad Sci USA* 109(50):20732–20737.
32. Taelman VF, et al. (2010) Wnt signaling requires sequestration of glycogen synthase kinase 3 inside multivesicular endosomes. *Cell* 143(7):1136–1148.
33. Khandjian EW, et al. (1998) Novel isoforms of the fragile X related protein FXR1P are expressed during myogenesis. *Hum Mol Genet* 7(13):2121–2128.
34. Luttrell LM, Gesty-Palmer D (2010) Beyond desensitization: Physiological relevance of arrestin-dependent signaling. *Pharmacol Rev* 62(2):305–330.
35. Hong LJ, et al. (January 24, 2015) Valproic acid influences MTNR1A intracellular trafficking and signaling in a beta-Arrestin 2-dependent manner. *Mol Neurobiol*, 10.1007/s12035-014-9085-y.
36. Phiel CJ, et al. (2001) Histone deacetylase is a direct target of valproic acid, a potent anticonvulsant, mood stabilizer, and teratogen. *J Biol Chem* 276(39):36734–36741.
37. Dalgard CL, Van Quill KR, O'Brien JM (2008) Evaluation of the in vitro and in vivo antitumor activity of histone deacetylase inhibitors for the therapy of retinoblastoma. *Clin Cancer Res* 14(10):3113–3123.
38. Orford K, Crockett C, Jensen JP, Weissman AM, Byers SW (1997) Serine phosphorylation-regulated ubiquitination and degradation of beta-catenin. *J Biol Chem* 272(40):24735–24738.
39. Aitken A, et al. (1984) Amino acid sequence at the site on protein phosphatase inhibitor-2, phosphorylated by glycogen synthase kinase-3. *Biochim Biophys Acta* 790(3):288–291.
40. Hnasko TS, et al. (2006) Cre recombinase-mediated restoration of nigrostriatal dopamine in dopamine-deficient mice reverses hypophagia and bradykinesia. *Proc Natl Acad Sci USA* 103(23):8858–8863.
41. Cook D, et al. (2011) Fragile X related protein 1 clusters with ribosomes and messenger RNAs at a subset of dendritic spines in the mouse hippocampus. *PLoS One* 6(10):e26120.
42. Colantuoni C, et al. (2011) Temporal dynamics and genetic control of transcription in the human prefrontal cortex. *Nature* 478(7370):519–523.
43. Caprara GV, Steca P, Cervone D, Artistico D (2003) The contribution of self-efficacy beliefs to dispositional shyness: On social-cognitive systems and the development of personality dispositions. *J Pers* 71(6):943–970.
44. Foland-Ross LC, et al. (2010) Amygdala reactivity in healthy adults is correlated with prefrontal cortical thickness. *J Neurosci* 30(49):16673–16678.
45. Leppänen JM (2006) Emotional information processing in mood disorders: A review of behavioral and neuroimaging findings. *Curr Opin Psychiatry* 19(1):34–39.
46. Phiel CJ, Wilson CA, Lee VM, Klein PS (2003) GSK-3alpha regulates production of Alzheimer's disease amyloid-beta peptides. *Nature* 423(6938):435–439.
47. Siomi MC, Zhang Y, Siomi H, Dreyfuss G (1996) Specific sequences in the fragile X syndrome protein FMR1 and the FXR proteins mediate their binding to 60S ribosomal subunits and the interactions among them. *Mol Cell Biol* 16(7):3825–3832.
48. Mientjes EJ, et al. (2004) Fxr1 knockout mice show a striated muscle phenotype: Implications for Fxr1p function in vivo. *Hum Mol Genet* 13(13):1291–1302.
49. Cook D, et al. (2014) FXR1P limits long-term memory, long-lasting synaptic potentiation, and de novo GluA2 translation. *Cell Reports* 9(4):1402–1416.
50. Garnon J, et al. (2005) Fragile X-related protein FXR1P regulates proinflammatory cytokine tumor necrosis factor expression at the post-transcriptional level. *J Biol Chem* 280(7):5750–5763.
51. Pickard BS (2015) Schizophrenia biomarkers: Translating the descriptive into the diagnostic. *J Psychopharmacol* 29(2):138–143.
52. Munkholm K, Vinberg M, Vedel Kessing L (2013) Cytokines in bipolar disorder: A systematic review and meta-analysis. *J Affect Disord* 144(1-2):16–27.
53. Pae CU, Lee KU, Han H, Serretti A, Jun TY (2004) Tumor necrosis factor alpha gene-G308A polymorphism associated with bipolar I disorder in the Korean population. *Psychiatry Res* 125(1):65–68.
54. Neale BM, Sklar P (2015) Genetic analysis of schizophrenia and bipolar disorder reveals polygenicity but also suggests new directions for molecular interrogation. *Curr Opin Neurobiol* 30:131–138.
55. Doherty JL, Owen MJ (2014) Genomic insights into the overlap between psychiatric disorders: Implications for research and clinical practice. *Genome Med* 6(4):29.
56. Leng Y, et al. (2008) Synergistic neuroprotective effects of lithium and valproic acid or other histone deacetylase inhibitors in neurons: Roles of glycogen synthase kinase-3 inhibition. *J Neurosci* 28(10):2576–2588.
57. Beaulieu JM, et al. (2008) Role of GSK3 beta in behavioral abnormalities induced by serotonin deficiency. *Proc Natl Acad Sci USA* 105(4):1333–1338.
58. Franklin KBJ, Paxinos G (2008) *The Mouse Brain in Stereotaxic Coordinates* (Academic Press, New York), 3rd Ed.
59. Bohn LM, et al. (1999) Enhanced morphine analgesia in mice lacking beta-arrestin 2. *Science* 286(5449):2495–2498.
60. Ahmad S, Fowler LJ, Whitton PS (2004) Effect of acute and chronic lamotrigine on basal and stimulated extracellular 5-hydroxytryptamine and dopamine in the hippocampus of the freely moving rat. *Br J Pharmacol* 142(1):136–142.
61. Beaulieu JM, Sotnikova TD, Gainetdinov RR, Caron MG (2006) Paradoxical striatal cellular signaling responses to psychostimulants in hyperactive mice. *J Biol Chem* 281(43):32072–32080.
62. Gainetdinov RR, et al. (1999) Role of serotonin in the paradoxical calming effect of psychostimulants on hyperactivity. *Science* 283(5400):397–401.
63. Stambolic V, Woodgett JR (1994) Mitogen inactivation of glycogen synthase kinase-3 beta in intact cells via serine 9 phosphorylation. *Biochem J* 303(Pt 3):701–704.
64. Scheid MP, Marignani PA, Woodgett JR (2002) Multiple phosphoinositide 3-kinase-dependent steps in activation of protein kinase B. *Mol Cell Biol* 22(17):6247–6260.
65. Kirkpatrick LL, McIlwain KA, Nelson DL (2001) Comparative genomic sequence analysis of the FXR gene family: FMR1, FXR1, and FXR2. *Genomics* 78(3):169–177.
66. First MB, Donovan S, Frances A (1996) Nosology of chronic mood disorders. *Psychiatr Clin North Am* 19(1):29–39.

67. Wechsler D, Matarazzo JD (1972) Wechsler's Measurement and *Appraisal* of *Adult Intelligence* (Williams & Wilkins, Baltimore, MD), 5th Ed, pp x, 572.
68. Hollingshead AdB, Redlich FC (1958) *Social Class and Mental Illness; A Community Study* (Wiley, New York), pp ix, 442.
69. Oldfield RC (1971) The assessment and analysis of handedness: The Edinburgh inventory. *Neuropsychologia* 9(1):97–113.
70. Blasi G, et al. (2009) Functional variation of the dopamine D2 receptor gene is associated with emotional control as well as brain activity and connectivity during emotion processing in humans. *J Neurosci* 29(47):14812–14819.
71. Blasi G, et al. (2009) Preferential amygdala reactivity to the negative assessment of neutral faces. *Biol Psychiatry* 66(9):847–853.
72. Taurisano P, et al. (2013) DAT by perceived MC interaction on human prefrontal activity and connectivity during emotion processing. *Soc Cogn Affect Neurosci* 8(8):855–862.
73. Lo Bianco L, et al. (2013) Interaction between catechol-O-methyltransferase (COMT) Val158Met genotype and genetic vulnerability to schizophrenia during explicit processing of aversive facial stimuli. *Psychol Med* 43(2):279–292.
74. Tottenham N, et al. (2009) The NimStim set of facial expressions: Judgments from untrained research participants. *Psychiatry Res* 168(3):242–249.
75. Friston KJ, Zarahn E, Josephs O, Henson RN, Dale AM (1999) Stochastic designs in event-related fMRI. *Neuroimage* 10(5):607–619.
76. McCrae RR, Costa PT, Jr (1987) Validation of the five-factor model of personality across instruments and observers. *J Pers Soc Psychol* 52(1):81–90.

Supporting Information

Del'Guidice et al. 10.1073/pnas.1506491112

SI Methods

Experimental Animals. C57BL/6J mice were obtained from Jackson Laboratory. βARR2-KO and GSK3β-Flox mice were described previously (24, 59). Mice were genotyped at weaning by PCR amplification of genomic DNA obtained from ear punch biopsies. All genotypes were determined at weaning and reconfirmed after experimentation. For all experiments, respective WT littermates were used as controls for KO mice, and all mice were 3–4 mo of age. Before the experiments, mice were housed 4–5 per cage in a humidity-controlled room at 23 °C on a 12 h light–dark cycle with ad libitum access to food and water. For chronic drug treatment involving subsequent behavioral scoring, mice were housed in the behavior test room for the duration of treatment. The Université Laval Institutional Animal Care Committee approved all experimental procedures in line with guidelines from the Canadian Council on Animal Care.

Drug Administration. For chronic treatments, sodium valproate (Sigma-Aldrich) was administered for a period of 21 d in chow at a concentration of 10 (VAL 10) or 25 (VAL 25) g per 1 kg of chow as described (56). For both VAL 10 and VAL 25, chow was hydrated before being administered to mice. Chow was replaced daily. Lithium chloride (Sigma-Aldrich) was added to the drinking water for a period of 15 d at a concentration of 0.12% wt/vol as described (8). Lamotrigine was injected daily 10 mg/kg (i.p.) for a period of 21 d as described (60). The inhibitor of HDAC1 MS275 (Exclusive Chemistry) was dissolved in a restricted minimal volume of DMSO and brought to the final concentration with distilled water. MS275 was chronically administrated for 21 d at 20 mg/kg (one i.p. injection daily) as described (37). For all chronic conditions, experiments were carried out 5 h after treatment cessation. For acute treatments, lithium chloride and sodium valproate were dissolved in saline and injected (i.p.). TDZD-8 (Calbiochem) and SL327 (Tocris Cookson Inc.) were injected (i.p.) after suspension in a minimal amount of Tween and brought to the final volume with distilled water as described (8, 61).

Antibodies. The anti–β-catenin, anti–phospho-GSK3β (Ser9), anti–phospho-CREB, anti-CREB, anti–phospho-JNK3, anti-JNK3, anti-p44/42, anti–phospho-p44/42 ERK, and anti-DARPP32 mouse monoclonal antibodies were purchased from Cell Signaling Technology. Anti–phospho-DARPP32 (Th34) rabbit polyclonal antibody was from Phosphosolutions. Anti–total-GSK3α/β clone 0011-A monoclonal antibody and anti–phospho-AKT (Thr308) polyclonal antibody were from Santa Cruz Biotechnology. Anti–total-AKT monoclonal antibody was obtained from Biosources. The anti-actin clone c4 monoclonal and the anti-FXR1P clone 6BG10 antibodies were from Chemicon/Milipore. The anti-FXR1P ML-12 polyclonal antibody (33) was a kind gift of Dr. E. R. Khanndjian (Laval University, Québec, Canada).

Immunoblots. Euthanasia and immunoblot analyses were performed as described (21). Briefly, mice were killed by cervical dislocation, after which the heads of animals were immediately cooled by immersion in liquid nitrogen for 6 s. The right hemistriatum and hemifrontal cortex were rapidly dissected out (within 30 s) on an ice-cold surface and frozen in liquid nitrogen before protein extraction. Tissue samples were homogenized in boiling 1% SDS solution and boiled for 5 min. Protein concentration was measured by using a DC-protein assay (Bio-Rad). Protein extracts (25 or 50 μg) were separated on precast 10% SDS/PAGE Tris-glycine gels (Life Technology) and transferred to nitrocellulose membranes. Blots were immunostained overnight at 4 °C with primary antibodies. Immune complexes were revealed using appropriate IR dye-labeled secondary antibodies from Licor Biotechnology. Quantitative analyses of fluorescent IR dye signal were carried out using an Odyssey Imager (Licor Biotechnology). For quantification, actin was used as a loading control for the evaluation of total protein levels, whereas respective total protein signals were used as loading controls for each phosphoprotein signal. Results were further normalized to respective control conditions to allow for comparison between separate experiments. The gels shown in the figures correspond to representative experiments, where each lane corresponds to a separate animal. Separate gels are presented within separate frames, and apparent signals may not be directly comparable between gel pictures.

Measurement of Locomotor Activity. Locomotion was evaluated under illuminated conditions in an automated Omnitech Digiscan apparatus (AccuScan Instruments) after a 72-h period of habituation to the test room as described (62). Locomotor activity was measured in terms of the total distance traveled (horizontal activity) as described (21).

TST. Mice were tested for 6 min in a tail suspension apparatus (Med-Associates) as described (8, 23). Behavior was scored as time spent in immobility (in seconds) over the last 4 min of the test.

The DLET. The DLET was performed for a period of 5 min with mice placed initially at the center of the dark chamber as described (8, 26, 57). Tests were conducted using an automated open field activity setup with light/dark insert (Med-Associates) with the light compartment illuminated at 600 lx. For acute treatments, animals were weighed, tail-marked, and habituated to the test room for 72 h before testing. The total time spent in the dark and light compartments, the total distance traveled, and the delay to cross from the dark to the light chamber for the first time were used as parameters for analysis.

Cloning of FXR1P-cDNA. The full-length FXR1P cDNA was amplified using a mouse whole brain cDNA library with the following primers: sense 5′-AAAAAAGCTTCGCCACCATGGCGAGAGGATCTCACCATCACCATCACCATGAGCTGACGGTGGAGGTTC-3′; antisense 5′-CAGTTATGGATCCCGTGAAACACCATTCAGGA-3′. Primer sequences were deduced from variant 1 of the mouse FXR1P cDNA nucleotide sequence (National Center for Biotechnology Information reference sequence NM_001113188.1). Sense primer contained a Kozak consensus sequence and a His tag. PCR amplifications were conducted with the Bio-Rad iProof High-Fidelity DNA Polymerase kit. The generated 1.8-Kb amplicon was subcloned in frame downstream of a histidine tag sequence in a modified pcDNA3.1(+) expression vector to generate the phisFXR1P plasmid. Alternatively, the amplicon was also subcloned in frame downstream of a 3XHA-Tag to generate the 3xHA FXR1P plasmid. Both plasmids were sequenced to ensure accuracy.

Generating Stable Expression of His-Tagged FXR1P Fusion Protein in HEK293. HEK293 cells were grown in DMEM high glucose containing 10% (vol/vol) FBS, 100 μg/mL penicillin, and 100 IU/mL streptomycin. All cells were maintained at 37 °C with 5% CO_2. Linearized phisFXR1P plasmid was transfected in HEK293 cells in 10-cm dishes using the calcium phosphate method. About 16 h posttransfection, the medium was supplemented with neomycin

(500 μg/mL), and cells were grown for 7–10 d, exchanging the supplemented medium every day.

For experiments involving overexpression of activated GSK3β or AKT, stable cells were further transfected with 5 μg of HA-GSK3β-S9A (63) or HA-PKB T308D S473D (64) pcDNA3.1(+) vectors. The effect of kinase expression on phisFXR1P level was monitored 24 h after transfection.

For treatments of HEK293, SB216763 (Tocris Cookson Inc.), alsterpaullone (Sigma-Aldrich), TDZD-8, and SL327 were solubilized in DMSO and used at a concentration of 10 μM. Lithium chloride was dissolved in water and used at 2 mEq.

Purification His-Tag-FXR1P From HEK293 Cells. FXR1P-transfected HEK293 cells were rinsed and extracted with PBS1X at 4 °C, centrifuged at 15,000 rpm for 1 min using an Eppendorf 5424/5424R minifuge rotor, and homogenized in binding/wash buffer [100 mM Na-Phosphate, pH 8.0; 600 mM NaCl; 0,02% (vol/vol) Tween-20; 1% (vol/vol) Triton X-100] for 1 h at 4 °C. Extracts were incubated with 2 mg of His-Tag isolation Dynabeads (Life Technologies) for 10 min at 4 °C. Beads were collected by magnetic separation, washed four times with binding/wash buffer, and resuspended in 100 μL of His elution buffer [300 mM imidazole; 50 mM Na-Phosphate, pH 8.0; 300 mM NaCl; and 0.01% (vol/vol) Tween-20) for 5 min at 4 °C.

Preparation of Recombinant FXR1P. N-terminal His-tagged recombinant FXR1P fusion protein was expressed and purified as followed. The full-length FXR1P cDNA was amplified from phisFXR1P with the following primers: sense 5′-AAAACATATGATGGCGGAGCTGACGGTGGAGG TTC-3′; antisense 5′-AAAAGGATCCTTAATCACATCTTTTGCCTAGCCCATT-3′. The generated amplicon was subcloned into Nde I/Bam HI-digested pET16b plasmid (Addgene) to obtain a pEThisFXR1P vector. pEThisFXR1P plasmid was transformed in an *E. coli* BL21(DE3) strain. Recombinant protein expression was allowed for 6 h at room temperature following induction with 1 mM isopropyl β-D-1-thiogalactopyranoside. Pelleted bacteria were resuspended in lysis buffer: 20 mM Tris·HCl (pH 8), 1.5 M NaCl, 0.2% (vol/vol) Nonidet P-40, and 10 mM imidazole supplemented with protease inhibitors. Suspensions were lysed by sonication and cleared by centrifugation. The His-tagged fusion protein containing supernatants was incubated with Ni-NTA (Qiagen) and washed with the lysis buffer, and bound proteins were eluted with 250 mM imidazole again in lysis buffer. After elution, proteins were dialyzed against 20 mM Tris·HCl (pH 8) and 150 mM NaCl at 4 °C overnight.

Generation of Mutant FXR1P. For in vitro phosphorylation experiments, single serine to alanine mutations corresponding to the nine putative GSK3β phosphorylation sites were generated by PCR amplification using the pEThisFXR1P plasmid as a template. Primers used to generate each individual mutant are described in Table S1. A eukaryotic vector expressing a FXR1P variant lacking all putative GSK3β phosphorylation sites was also generated by this same method using the 3xHA FXR1P plasmid as a template.

Kinase Assay. Recombinant substrates (0.5 μg) were incubated with 0.1 μg of recombinant ERK (Promega) or GST-tagged GSK3β (Enzo Life Sciences) in assay buffer (20 mM Tris, pH 7.5; 10 mM $MgCl_2$; 5 mM DTT; 0.2 mM ATP; and 0.5 μCi of [γ^{32}P]ATP) for 10 min at 30 °C. Reactions were stopped by the addition of Laemmli loading buffer, boiled for 5 min, and resolved on 10% SDS/PAGE. Gels were stained with Coomassie blue, dried, and autoradiographed. Incorporation of ^{32}P on substrates was quantified from scanned autoradiograms using Image J (NIH).

To produce FXR1P', recombinant FXR1P produced in *E. coli* was incubated with recombinant ERK2 for 1 h at 37 °C, and reaction was stopped by the addition of the ERK inhibitor pyraz (Sigma-Aldrich) at a final concentration of 1 μM. For each batch of FXR1P′, a test kinase assay with [γ^{32}P]ATP was carried out without adding extra kinases to verify the full inhibition of ERK2 by the inhibitor. Absence of and effect of pyraz on GSK3β activity was assessed by kinase assay using recombinant phosphatase inhibitor 2 (New England Biolabs) as a priming independent GSK3β substrate (39).

Preparation of AAV Vector for Neuronal FXR1P Expression. Serotype 5 AAV particles were used for specific neuronal expression of recombinant GFP-FXR1P under the control of the synapsin (SYN) gene promoter. TheGFP-FXR1P construct was made using Gibson assembly (New England Biolabs). GFP and FXR1P were PCR amplified using the following primers: for GFP, sense 5′-GGCTAGCGTTTAAACTTAAGCTTGCCGCCACCATGGTGAGCAAGGGCGA-3′ and antisense 5′-CCAGCACTCTTGTACAGCTCGTCCATG-3′. For FXR1P, sense 5′-CTGTACAAGAGTGCTGGTGGTAGTGCTGGTGGTAGTGCTGGTGGTAGTGCTGGTGGTAGTGCTGGTGGTGCGGAGCTGACGGTGGA-3′ and antisense 5′-TGCTGGATATCTGCAGAATTCTTATGAAACACCATTCAGGACTGCT-3′. GFP and FXR1P fragments were cloned into KpnI- and BsrGI-digested pcDNA 3.1(+) using a Gibson assembly kit. To generate the pAAV hSYN GFP-FXR1P vector, GFP-FXR1P was amplified by PCR from the pcDNA GFP-FXR1P vector using the following primers: sense 5′-AATAATGGATCCGCCGCCACC ATGGTGAGCAAGGGCGAGGA-3′ and antisens 5′-AATAATGAATTCTTATGAAACACCATTCAGGACTGCT-3′. It was then cloned into pAAV hSYN EGFP (Addgene plasmid 50465) using BamHI EcoRI sites. rAAV hSYN EGFP was purchased from preexisting stocks from the University of North Carolina (UNC) vector core facility. The AAV vector expressing GFP-Cre (40) was a kind gift from Dr. Richard D. Palmiter (University of Washington, Seattle, WA). Infectious viral particles for all vectors were produced by the UNC Vector core facility.

Surgery. Twenty-one days before the behavioral tests, a bilateral injection of virus was made in the dmPFC with 10 animals per group. For surgical procedures, mice were anesthetized with a preparation of xylazine 5% + ketamine 10% + sterilized water (10 μL/1 g, i.p.). Then the animal was placed in a stereotaxic frame, and the skull surface was exposed. Two holes were drilled at appropriate sites corresponding to the coordinates of the dmPFC taken from the mouse brain atlas (58): anterior-posterior (AP), +2.7 mm anterior to bregma; lateral, ±0.5 mm; dorsoventral (DV), 1.6 mm below the skull. All measures were taken before, during, and after surgery to minimize animal pain and discomfort.

Statistical Analysis, in Vitro, and Animal Studies. The data are presented as means ± SEM. Data from Western blot were analyzed by two-tailed *t* test or ANOVA; behavioral data were evaluated by *t* test, or repeated measures two-way ANOVA or one way ANOVA followed by Bonferroni-corrected pair-wise comparisons using Prism 4.0c (GraphPad Software Inc.) for Macintosh computers. $P < 0.05$ was considered significant.

Human Subjects. All subjects included in the human study provided written informed consent to the study after the procedure was fully explained to them. The protocol was approved by the local Institutional Review Board.

Genotyping of Human Subjects. All participants in the study (see below for sample characteristics) underwent blood withdrawal for subsequent DNA extraction from peripheral blood mononuclear

cells. Approximately 200 ng DNA was used for genotyping analysis. DNA was concentrated at 50 ng/μL (diluted in 10 mM Tris/1 mM EDTA) with a Nanodrop Spectrophotometer (ND-1000). Illumina HumanHap550K/610Quad Bead Chips was used to genotype our sample. Briefly, each sample was whole-genome amplified, fragmented, precipitated, and resuspended in appropriate concentrations of hybridization buffer. Denatured samples were hybridized on prepared Illumina Human550K/610-Quad Bead Chips. After hybridization, the Bead Chip oligonucleotides were extended by a single labeled base, which was detected by fluorescence imaging with an Illumina Bead Array Reader. Normalized bead intensity data obtained for each sample were loaded into the Illumina GenomeStudio (Illumina, v.2010.1) with cluster position files provided by Illumina, and fluorescence intensities were converted into SNP genotypes. After genotypes were called and the pedigree file was assembled, we removed SNPs showing a minor allele frequency <1%, genotype missing rate >5%, or deviation from Hardy–Weinberg equilibrium ($P < 0.0001$). Individuals were also removed if their overall genotyping rate was below 97%. Sample duplications and cryptic relatedness were ruled out through identity-by-state analysis of genotype data.

To reduce sources of variability, a subsample of Braincloud dataset (braincloud.jhmi.edu) (42) including only Caucasian subjects with postnatal age and RNA integrity ≥7 ($N = 94$, 71 male; mean age, 30.5 ± 20.4; mean postmortem pH, 6.5 ± 0.2; RIN, 8.44 ± 0.5; PMI, 26.1 ± 14.3 h) was used.

FXR1 promoter was defined as described (65). Two SNPs, rs496250 and rs1805562, were identified within that region. The data of 94 subjects were available for rs496250 and rs1805562. Sample sizes as a function of genotype were as follows: rs1805562—A/A, 3; A/C, 31; C/C, 60; rs496250—G/G, 71; A/G, 17; A/A, 6. Because of the small number of subjects within the minor allele homozygous group, these subjects were grouped with the heterozygous in subsequent analyses (for rs1805562—A carrier, 34; C/C, 60; for rs496250—A carrier, 23; G/G, 71).

ANOVA was used to explore the association between SNPs in *FXR1* and *FXR1* expression as measured with the constitutive probe, detecting the full gene transcript. Given that Braincloud includes samples encompassing the entire life span, age and Age × Genotype interaction were included in the general linear model as covariates of no interest. Results were Bonferroni-corrected for the number of SNPs analyzed.

Functional Imaging Study.

Subjects. A total of 197 healthy subjects (102 males; mean age, 27.4 ± 7.5; mean IQ, 108.22 ± 11.84; Handedness, 0.78 ± 0.39) were enrolled in the study. All participants were white Caucasians from the region of Puglia, Italy. The Structured Clinical Interview for the Diagnostic and Statistical Manual of Mental Disorders (DSM- IV) (66) was used to exclude any axis I psychiatric disorder. Exclusion criteria were presence of any neurological or medical condition revealed by clinical and magnetic resonance imaging evaluation, presence of head trauma with loss of consciousness, and drug abuse within the past 6 mo. Furthermore, The Wechsler Adult Intelligence Scale–Revised was used to evaluate IQ (67), the Hollingshead Scale (68) to calculate the socioeconomic status, and the Edinburgh Inventory (69) to measure handedness.

After genotype determination, sample sizes as a function of genotype were as follows: *FXR1*—A/A, 8; A/G, 69; G/G, 120; *GSK3B*—GG, 64; GT, 96; TT, 37. As for the postmortem study and given the low number of subjects homozygous for the *FXR1* A allele, we collapsed these individuals and heterozygous subjects within one group, resulting in 24 *FXR1* A carrier/*GSK3B* GG; 41 *FXR1* A carrier/*GSK3B* GT, 12 *FXR1* A carrier/*GSK3B* TT, 40 *FXR1* GG/*GSK3β* GG, 55 *FXR1* GG/*GSK3B* GT, and 25 *FXR1* GG/*GSK3B* TT.

fMRI task. During fMRI, all subjects completed an event-related fMRI paradigm already used in previous fMRI studies (70–73). This paradigm consisted of a presentation of faces with angry, fearful, happy, and neutral emotional expressions from a validated set of facial pictures (NimStim, www.macbrain.org/resources.htm) (74). Subjects were asked to identify the sex of each face (perceptual processing of facial expressions; implicit processing). From stimulus appearance, 2 s were allowed for behavioral responses. Each stimulus was presented for 500 ms, with an interstimulus interval randomly jittered between 2 s and 7 s. The order of facial stimuli was pseudorandomized across the session (75). The stimuli used were pictures of faces with four different expressions. The total number of stimuli was 144: 30 angry, 39 fearful, 37 happy, and 38 neutral faces. A fixation cross-hair was presented during the interstimulus interval. The total duration of the task was 6 min and 8 s.

fMRI data acquisition and analysis. fMRI was performed on a GE Signa 3T scanner with a gradient echo-planar imaging sequence (repetition time, 2,000 ms; echo time, 28 ms; 26 interleaved slices, thickness of 4 mm, gap of 1 mm; voxel size, 3.75 × 3.75 × 5; scan repetitions, 180; flip angle, 90°; field of view, 24 cm; matrix, 64 × 64). The first four scans were discarded to allow for signal saturation. The visual stimuli were presented via a back-projection system using Presentation (Version 9.00, Neurobehavioral Systems).

Analysis of the fMRI data was completed using Statistical Parametric Mapping (SPM8; www.fil.ion.ucl.ac.uk/spm). Images for each subject were realigned to the first volume in the time series, and movement parameters were extracted to exclude subjects with excessive head motion (>2 mm of translation, >2° rotation). Images were then resampled to a 2-mm isotropic voxel size, spatially normalized into a standard stereotactic space (Montreal Neurological Institute, template) and smoothed using a 8-mm full-width half-maximum isotropic Gaussian kernel to minimize noise and to account for residual intersubject differences. A box car model convolved with the hemodynamic response function at each voxel was modeled. Vectors were created for angry, happy, fearful, and neutral faces. Residual movement was modeled as a regressor of no interest. Predetermined condition effects at each voxel were created using a *t* statistic, producing a statistical image for BOLD responses to brain processing of stimuli representative of each condition—that is, angry, happy, fearful, and neutral faces versus fixation cross-hair. ANCOVA with sex as covariate of no interest was then used at the group level to investigate the main effect of facial expressions, of *FXR1*, of *GSK3B*, as well as of their interactions. This analysis was constrained by a mask obtained by combining group activation maps associated with processing of each facial expression.

We used a statistical threshold of $P < 0.05$ and a minimum cluster size of [k] = 10, family-wise error-corrected using as volume of interest the amygdala, as identified with the Wake Forest University PickAtlas (fmri.wfubmc.edu/software/PickAtlas). This region was chosen a priori based on its deep involvement in processing of emotions and of emotionally charged facial expression (70–73). Significant BOLD responses were extracted using MarsBar (marsbar.sourceforge.net/).

Demographics and behavioral data analysis. ANOVAs and χ^2 were used as needed to assess potential differences between *FXR1* and *GSK3B* genotype groups for all demographic variables as well as for behavioral data. Post hoc analyses were performed with Fisher LSD.

Human Behavioral Study. A total of 153 healthy subjects (66 males; mean age, 27.57 ± 7.53; mean full IQ, 110.07 ± 11.47) were enrolled in this study. All participants were Caucasians from the region of Puglia, Italy. Exclusion criteria were the same as in the fMRI study. Sample sizes as a function of genotype were as follows: *FXR1*—A/A, 7; A/G, 49; G/G, 97; *GSK3B*—GG, 58; GT, 70; TT, 25. As for the postmortem study and given the low number of subjects homozygous for the *FXR1* A allele, we

collapsed these individuals and heterozygous subjects within one group, resulting in 18 *FXR1* A carrier/*GSK3B* GG, 32 *FXR1* A carrier/*GSK3B* GT, 6 *FXR1* A carrier/*GSK3B* TT, 40 *FXR1* GG/*GSK3B* GG, 38 *FXR1* GG/*GSK3B* GT, and 19 *FXR1* GG/*GSK3B* TT.

All subjects completed the BFQ (43), measuring the Big Five Factors Model (76). This questionnaire includes five dimensions (energy, friendliness, conscientiousness, emotional stability, and openness). Here, we have focused on emotional stability, which refers to the tendency to experience negative feelings (43). In particular, individuals with low scores on emotional stability often experience emotional instability and negative emotions such as anxiety, depression, or anger (43).

ANOVA and χ^2 test were used to assess potential differences between genotype groups for all demographic variables. Furthermore, factorial ANOVA was used to investigate the main effect of each genotype and their interaction on emotional stability. Post hoc analyses were performed with Fisher LSD.

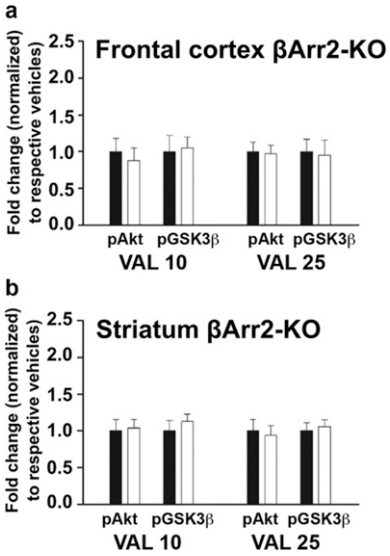

Fig. S1. Effects of VAL 10 and VAL 25 treatments on GSK3β phosphorylation are dependent on βArrestin2 expression. (*A* and *B*) Quantitative immunoblot analysis of pAKT and pGSK3β in the frontal cortex (*A*) and striatum (*B*) of βARR2-KO following chronic VAL 10 and VAL 25 treatments. Data are means ± SEM.

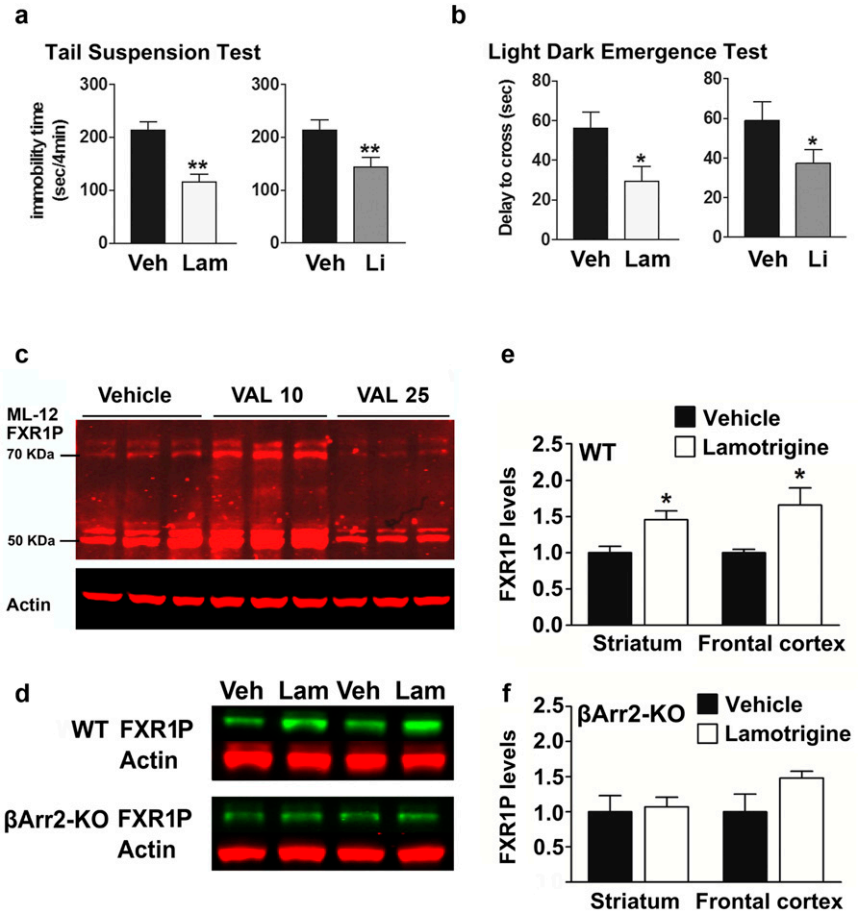

Fig. S2. Levels of FXR1P are regulated differentially by VAL 10 and VAL 25 and lamotrigine. (*A* and *B*) TST (*A*) and DLET (*B*) showing behavioral effects of chronic lithium and lamotrigine treatment in WT mice. Data are means ± SEM. $*P \leq 0.05$, $**P \leq 0.01$, $***P \leq 0.005$. One-way ANOVA with Bonferroni-corrected pairwise comparisons was performed; $n = 10$ mice per group. (*C*) Further validation of changes of frontal cortex FXR1P levels following treatment of C57Bl6 mice with the VAL 10 and VAL 20 doses regimens. The ML-12 antibody detected a 70-KDa and a 50-KDa band cluster. Notably both clusters were equally affected by treatment. (*D*–*F*) Quantitative immunoblot analysis of FXR1P levels in extracts prepared from the frontal cortex of WT and βARR2-KO littermates after chronic treatment with lamotrigine (10 mg/kg i.p., 21 d).

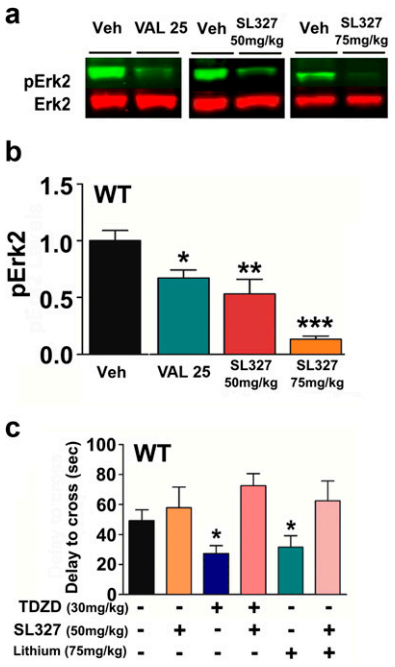

Fig. S3. Inhibition of ERK antagonizes the effects of GSK-3 inhibition in the DLET. (*A* and *B*) Quantitative immunoblot analysis of pERK2 levels in the striatum of WT C57Bl6 mice treated acutely with the MEK inhibitor SL327 or chronically with the VAL 25 dose regimen. Data (means ± SEM) were normalized to average protein levels in vehicle-treated animals from the same genotype. $*P \leq 0.05$, $**P \leq 0.01$, $***P \leq 0.005$. Student double-tailed *t* test was performed (drug vs. vehicle within each genotype). $n = 5$ mice per group. (*C*) DLET for WT C57Bl6 mice treated with TDZD-8, SL327, and/or LiCl. Behavior was scored as latency to first cross to the illuminated (light) compartment. Data are means ± SEM. $*P \leq 0.05$. One-way ANOVA with Bonferroni-corrected pairwise comparisons was used; $n = 10$ mice per group.

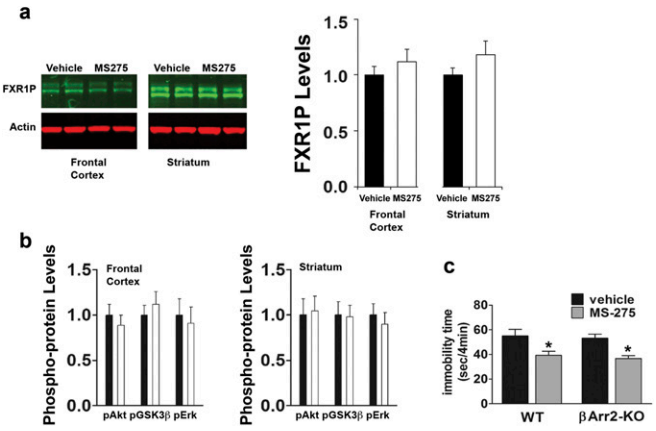

Fig. S4. Inhibition of HDAC1 does not affect FXR1P levels. (*A*) Quantitative immunoblot analysis of FXR1P relative levels in the frontal cortex and striatum of WT mice following chronic administration of the HDAC1 inhibitor MS275. Data are means ± SEM and are normalized to the vehicle-treated group. $n = 5$ mice per group. (*B*) Quantitative immunoblot analysis of pAKT, pGSK3β, and pErk2 in the frontal cortex and striatum of WT mice following chronic administration of MS275. Data are means ± SEM and are normalized to the vehicle-treated group. $n = 5$ mice per group. (C) TST for βARR2-KO and WT littermates following chronic administration of MS275. Behavior was scored for the last 4 min of the test. Data are means ± SEM. $*P \leq 0.05$. One-way ANOVA with Bonferroni-corrected pairwise comparisons was used; $n = 10$ mice per group.

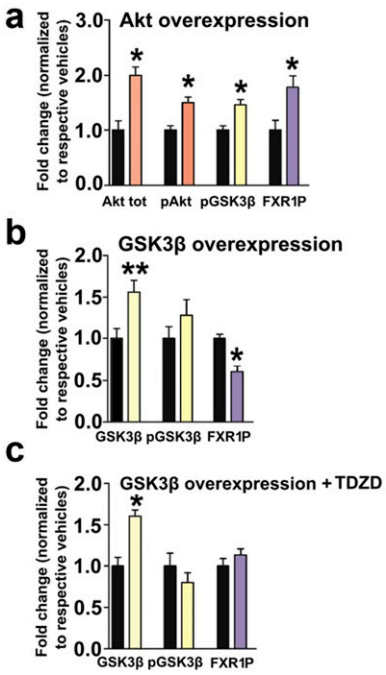

Fig. S5. Inhibition of ERK antagonizes the effects of GSK3 inhibition. (*A*–*C*) Quantitative immunoblot analysis of protein and/or phosphoprotein levels in stably transfected HEK293 cells expressing his-tagged recombinant mouse FXR1P. (*A*) Cells were further transfected with a vector expressing a constitutively active Akt1 mutant. (*B*) Cells were further transfected with a vector expressing a constitutively active GSK3β mutant. (*C*) Cells expressing constitutively active GSK3β were further treated with TDZD8 (10 μM, 60 min). Black bars correspond to control vehicle conditions. Respective total protein signal was used as the internal reference for phosphoproteins. Actin was used as a reference for the measurement of changes in the relative levels of a given protein. Data (means ± SEM) were normalized to average protein levels in vehicle-treated cells. $*P \leq 0.05$, $**P \leq 0.01$, $***P \leq 0.005$. Student double-tailed *t* test was performed (drug vs. vehicle within each genotype). $n = 5$ separate cell cultures. Detection and quantification of immunoblot signal were performed within a linear signal range using near-infrared fluorescence and a LiCor Odyssey.

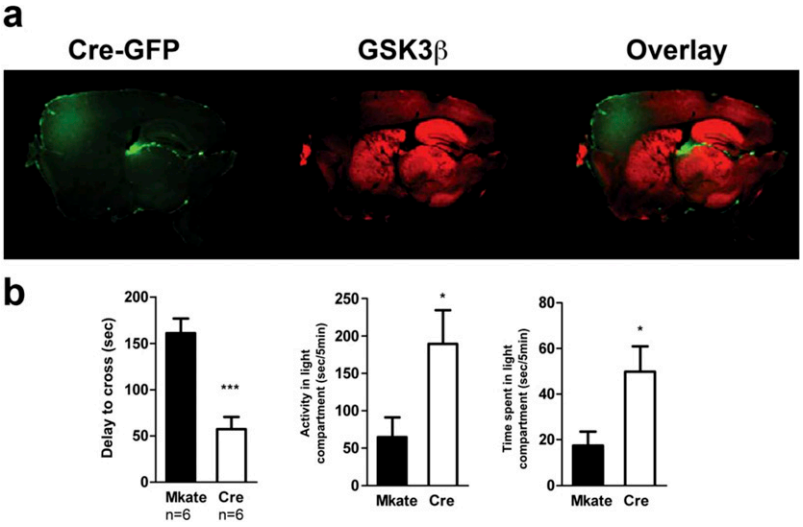

Fig. S6. AAV-Cre–mediated inactivation of GSK3β replicates the effect of VAL 10 treatment in the DLET. (*A*) Tissue sections from GSK3β flox mice infected with an AAV vector expressing a GFP-tagged Cre recombinase at 3 wk after infection. Cre-GFP (green) was detected using an anti-GFP polyclonal antibody and GSK3β (red) a monoclonal anti-GSK3 antibody. Images were acquired by direct scanning using the Odyssey Imager at a resolution of 21 μm. (*B*) Cre-GFP–mediated inactivation of GSK3β replicates behavioral effects of valproate and lithium in the DLETs. GSK3β Flox mice were injected with either AAVmKate control virus or AAVCre-GFP virus and tested 3 wk after viral injection. Data are means ± SEM. $*P \leq 0.05$. One-way ANOVA with Bonferroni-corrected pairwise comparisons was used; $n = 10$ mice per group. Data are means ± SEM. $*P \leq 0.05$, $**P \leq 0.01$, $***P \leq 0.005$. One-way ANOVA with Bonferroni-corrected pairwise comparisons was used; $n = 10$ mice per group.

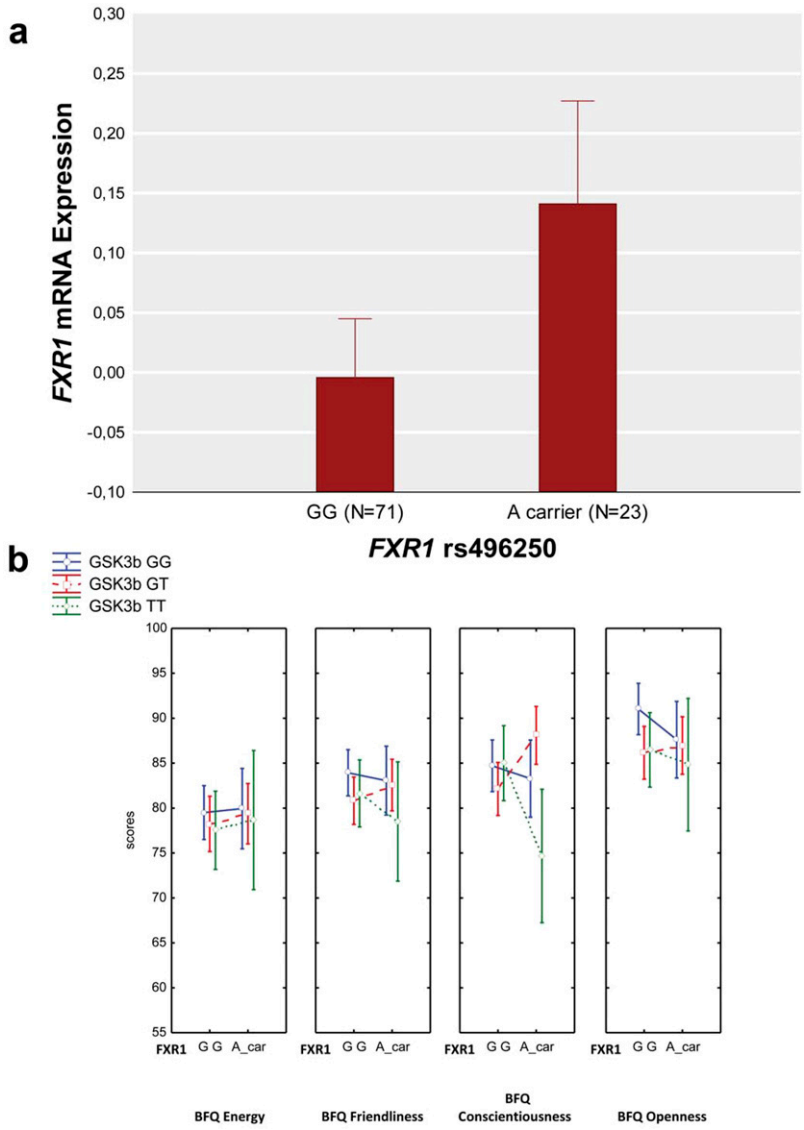

Fig. S7. Effect of rs496250 genotype on postmortem brain FXR1 gene expression (mRNA) and selectivity of *FXR1 GSK3B* interaction on the BFQ. (*A*) Subjects carrying the A allele for rs496250 have statistically significant greater expression levels of *FXR1*. Histogram depicts normalized log2 ratios (sample/reference). Data are from braincloud.jhmi.edu/. (*B*) No Interaction between *FXR1* rs496250 and *GSK3β* rs12630592 on other dimensions of the BFQ. Data are means ± SEM.

Table S1. Forward PCR primers used for FXR1P site-directed mutagenesis

Mutated site	Mutation	Forward primer, 5′ to 3′
Site 1	S308A	GACAGATTGGTGCTAGGTCTTATAGTGGAAG
Site 2	S397A	TTACACCGCCGGTTATGGTACAAATTCTGAGC
Site 3	S409A	TGTCTAACCCCGCCGAAACAGA
Site 4	S463A	CAAAGCCTCCATCAGTTCTGTGC
Site 5	S474A	AAAGATCCAGACGCCAATCCATACAG
Site 6	S496A	GCCAGCGAAGCTCACCACAGTA
Site 7	T522A	GTTCTGATGGATGGACTGGCTGAA
Site 8	S524A	AGCTGATACAGCCTCAGTTAATGAGAATGGG
Site 9	S542A	AGTTGCAGATTATATTGCTAGAGCTGAGTCTC

All reverse primers are the respective reverse complement.